REPORT

PROTEOSTASIS

UBE2O is a quality control factor for orphans of multiprotein complexes

Kota Yanagitani,* Szymon Juszkiewicz, Ramanujan S. Hegde†

Many nascent proteins are assembled into multiprotein complexes of defined stoichiometry. Imbalances in the synthesis of individual subunits result in orphans. How orphans are selectively eliminated to maintain protein homeostasis is poorly understood. Here, we found that the conserved ubiquitin-conjugating enzyme UBE2O directly recognized juxtaposed basic and hydrophobic patches on unassembled proteins to mediate ubiquitination without a separate ubiquitin ligase. In reticulocytes, where UBE2O is highly up-regulated, unassembled α-globin molecules that failed to assemble with β-globin were selectively ubiquitinated by UBE2O. In nonreticulocytes, ribosomal proteins that did not engage nuclear import factors were targets for UBE2O. Thus, UBE2O is a self-contained quality control factor that comprises substrate recognition and ubiquitin transfer activities within a single protein to efficiently target orphans of multiprotein complexes for degradation.

Cells have evolved a wide range of quality control pathways to monitor failures in protein biogenesis and promptly target defective products for degradation (*1*, *2*). Ineffective quality control is implicated in aging and can cause neurodegeneration (*3*); conversely, robust quality control may be especially crucial in cancer to support high rates of protein synthesis in the face of an aberrant genome and environmental stresses (*4*). The suite of protein quality control pathways needed for cellular homeostasis in metazoans is incompletely defined (*1*).

To identify additional cytosolic quality control pathways, we sought an aberrant protein whose ubiquitination in a cell-free cytosolic extract occurs without engaging known quality control factors. A transmembrane (TM) domain interrupted by three basic residues (hereafter termed 3R) (fig. S1A) is not recognized by quality control factors specialized for mislocalized membrane proteins, such as BAG6 or the ubiquilin family members (*5*–*7*); yet, 3R was ubiquitinated similarly to a BAG6 substrate (fig. S1B). Although 3R is an artificial mutant, we reasoned that mechanistic dissection of its ubiquitination pathway might lead us to a quality control pathway and provide tools that could be exploited to identify physiological substrates.

In vitro–translated ^{35}S-labeled 3R immunopurified under native conditions became modified with His-ubiquitin in the presence of recombinant E1, E2 (UBCH5), and adenosine 5′-triphosphate (ATP) (fig. S1, C and D), indicating that the immunopurified complexes contained a ubiquitin ligase. The primary 3R-associated ubiquitination activity had a native molecular weight of ~150 to 300 kD (Fig. 1, A and B). Cross-linking reactions of the active fractions revealed interacting partners of ~200, ~120, and ~100 kD (Fig. 1B). Mass spectrometry identified UBE2O as the ~200-kD product, Importin 5 (IPO5) and Importin 7 (IPO7) as the 120-kD product, and Importin β as the ~100-kD product (fig. S2A). Although none of these are ubiquitin ligases, UBE2O is a ubiquitin-conjugating (E2) enzyme, with suspected ubiquitin transfer capability (*8*). Furthermore, UBE2O is up-regulated in cells in response to induced misfolding of a cytosolic protein (*9*). We thus investigated its potential role in recognition and ubiquitination of 3R and other aberrant proteins.

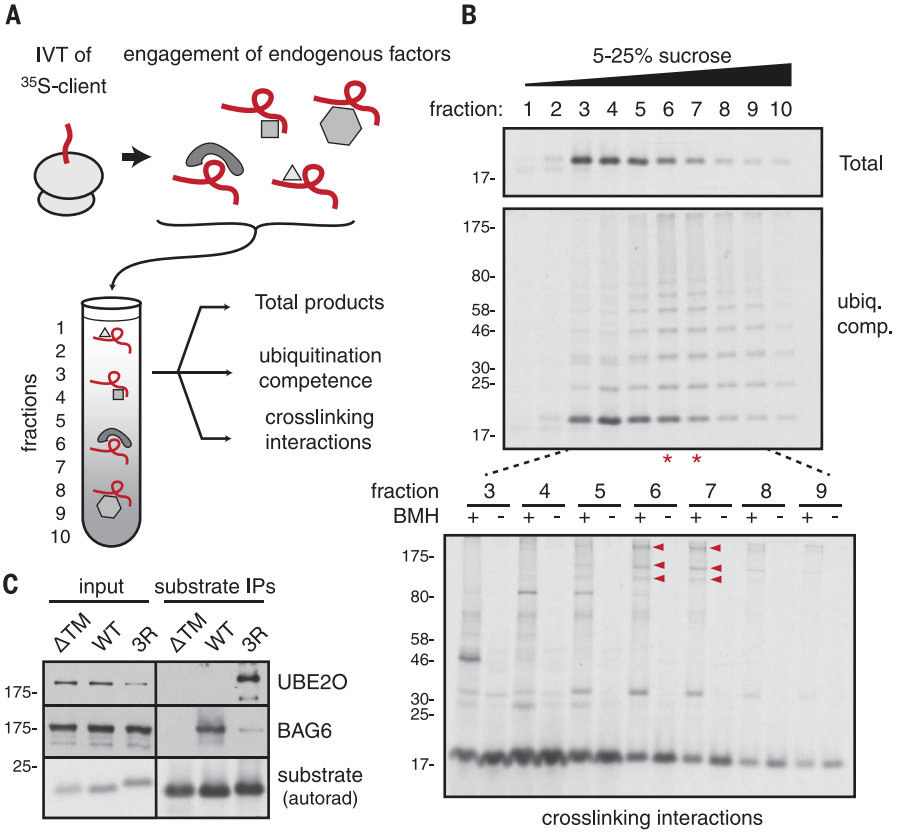

Fig. 1. UBE2O associates with an aberrant nascent protein in the cytosol. (**A**) Experimental strategy to identify quality control factors through cross-correlation of native size, physical interactors, and ubiquitination activity. (**B**) ^{35}S-labeled Sec61β(3R) was translated in reticulocyte lysate (RRL) for 15 min, which is just long enough to synthesize the proteins but before appreciable downstream ubiquitination. The reaction was separated according to native size on a sucrose gradient, and each fraction was analyzed for ubiquitination competence (middle) or physical interactions (bottom). Red asterisks indicate fractions with peak ubiquitination activity, and red arrowheads indicate cross-linked proteins with a peak in these same fractions. (**C**) Sec61β wild type (WT) or mutants lacking the transmembrane domain (ΔTM) or containing 3R were translated in RRL, immunoprecipitated under native conditions, and analyzed by means of immunoblotting for either BAG6 or UBE2O. BAG6 interacts with the intact TM domain, whereas UBE2O preferentially interacts with the 3R-disrupted TM domain.

Immunoblotting of natively immunopurified 3R verified its interaction with UBE2O. By contrast, BAG6 interacted efficiently with an intact TM domain but poorly with 3R (Fig. 1C), which is consistent with its preference for long uninterrupted hydrophobic domains (*5*, *10*). Immunoprecipitation of cross-linking reactions verified that the ~200-kD cross-linking partner from Fig. 1B was indeed UBE2O, suggesting a direct interaction with 3R (fig. S2B). Furthermore, the small globular protein KRAS did not interact with UBE2O, whereas mutants designed to disrupt its folding (termed K1 and K2) showed increased ubiquitination and UBE2O interaction (fig. S3, A to C). Given that UBE2O was observed prominently in stained gels of affinity-purified samples (figs. S2A and S3D), we conclude it is a major and relatively stable interactor, with selectivity for aberrant proteins such as 3R and misfolded KRAS.

Experiments with purified recombinant factors demonstrated that UBE2O is sufficient for interaction with and ubiquitination of its clients. We first synthesized 3R in a "PURE" (protein synthesis using recombinant elements) in vitro translation system reconstituted from recombinant *Escherichia coli* translation factors (*11*). Nascent 3R normally precipitates in this chaperone-free PURE system but was prevented from aggregation by including Calmodulin (CaM) during the translation (fig. S4A). CaM acts as a chaperone for hydrophobic domains (*12*) and can be induced to retain or release 3R by using Ca^{2+} or EGTA, respectively. Cross-linking assays verified that purified UBE2O (fig. S4B) engaged 3R released from CaM with EGTA but not with the CaM-3R complex (Fig. 2, A and B). In this system, UBE2O (together with E1, ubiquitin, and ATP) was sufficient for 3R ubiquitination (Fig. 2C), whereas the promiscuous E2 enzyme UBCH5 was ineffective toward 3R on its own (Fig. 2C and fig. S5A).

Ubiquitination required the TM-3R region and was markedly impaired if release from CaM was inhibited with excess Ca^{2+} (Fig. 2C). Other hydrophobic regions could also be directly recognized and ubiquitinated by UBE2O in this purified system (fig. S5B), even though they would be recognized by other factors (such as BAG6) in a complete cytosol (*5*, *7*, *12*). The maximal number of ubiquitins added to the client corresponded to the number of available primary amines and was not affected appreciably by using methyl-ubiquitin incapable of forming polyubiquitin chains (fig. S5C). C1040 in the E2 domain of UBE2O was essential for ubiquitination activity (Fig. 2D) but not for interaction with a client. Of the conserved regions (CR) of UBE2O (*13*), deletion of CR2, and to a lesser extent CR1, reduced client ubiquitination without affecting UBE2O activity, as judged by auto-ubiquitination (Fig. 2D). Correspondingly, recombinant CR2, and to a lesser extent CR1, could

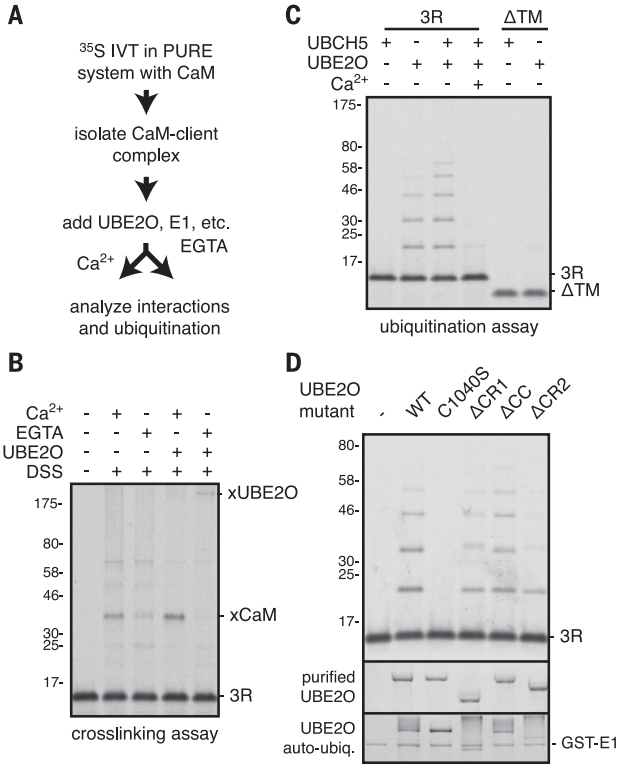

Fig. 2. Reconstitution of UBE2O-mediated client ubiquitination with purified factors. (**A**) Experimental strategy to test UBE2O interaction and ubiquitination in a defined system. (**B**) ^{35}S-labeled 3R in complex with CaM was treated with either Ca^{2+} or EGTA in the presence or absence of UBE2O and subjected to the amine-reactive cross-linker disuccinimidyl suberate (DSS). Positions of the starting 3R substrate and its cross-links to CaM (xCaM) and UBE2O (xUBE2O) are indicated. (**C**) ^{35}S-labeled 3R in complex with CaM was mixed with E1, ATP, ubiquitin, and the indicated E2 (UBCH5 or UBE2O), then treated with EGTA so as to induce substrate release from CaM. One sample was incubated with Ca^{2+} instead of EGTA. (**D**) Ubiquitination reactions as in (C), with the indicated UBE2O variants. The purified UBE2O proteins before and after the ubiquitination reaction are also shown to indicate auto-ubiquitination of UBE2O in all reactions except with the C1040S mutant. (Single-letter abbreviations for the amino acid residues are as follows: A, Ala; C, Cys; D, Asp; E, Glu; F, Phe; G, Gly; H, His; I, Ile; K, Lys; L, Leu; M, Met; N, Asn; P, Pro; Q, Gln; R, Arg; S, Ser; T, Thr; V, Val; W, Trp; and Y, Tyr. In the mutants, other amino acids were substituted at certain locations; for example, C1040S indicates that cysteine at position 1040 was replaced by serine.)

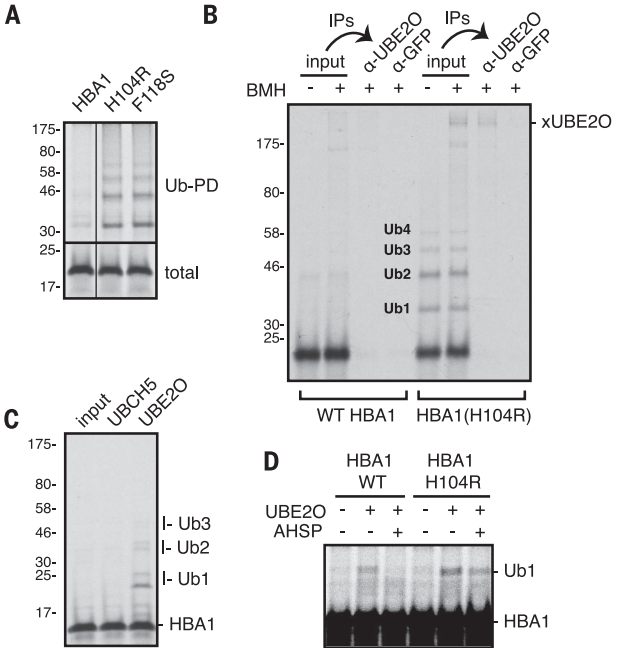

Fig. 3. Unassembled α-globin is a target for UBE2O ubiquitination. (**A**) Wild-type α-globin (HBA1) or two assembly mutants (H104R and F118S) were translated in RRL supplemented with His-tagged ubiquitin and either analyzed directly (bottom; total) or after ubiquitin-pulldown (Ub-PD) via the His tag (top). (**B**) Hemagglutinin (HA)–tagged HBA1 or the H104R mutant were translated in RRL, subjected to sulfhydryl-reactive cross-linking with bismaleimidohexane, and affinity-purified via the HA tag. The purified products were denatured and analyzed directly (input) or further immunoprecipitated with antibodies to either UBE2O or GFP. The positions of ubiquitinated H104R and its cross-link to UBE2O are indicated. (**C**) ^{35}S-labeled HBA1 synthesized in the PURE translation system was incubated with E1, ATP, ubiquitin, and either UBCH5 or UBE2O and analyzed for ubiquitination. (**D**) ^{35}S-labeled WT or H104R mutant HBA1 synthesized in the PURE system was incubated with or without UBE2O and AHSP as indicated. The positions of unmodified and ubiquitinated HBA1 are indicated.

Medical Research Council (MRC) Laboratory of Molecular Biology, Francis Crick Avenue, Cambridge Biomedical Campus, Cambridge, CB2 0QH, UK.
*Present address: The Thomas N. Sato BioMEC-X Laboratories, Advanced Telecommunications Research Institute International (ATR), Hikaridai 2-2-2, Kyoto 619-0288, Japan. †Corresponding author. Email: rhegde@mrc-lmb.cam.ac.uk

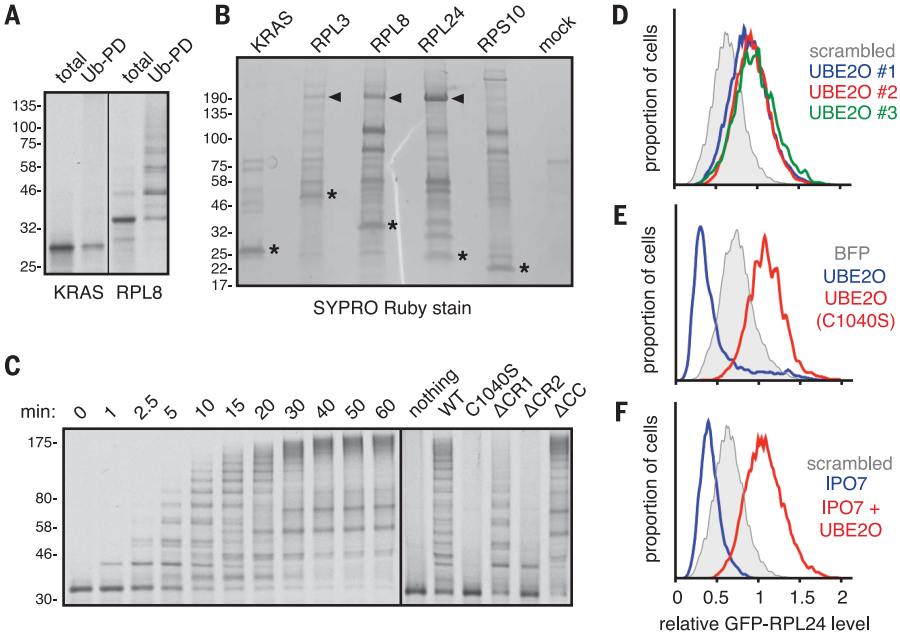

Fig. 4. UBE2O facilitates degradation of cytosolic orphan ribosomal proteins. (**A**) Wild-type KRAS or RPL8 was translated in RRL supplemented with His-tagged ubiquitin and either analyzed directly (total) or after ubiquitin-pulldown (Ub-PD) via the His tag. (**B**) The indicated FLAG-tagged proteins were translated in RRL, affinity-purified under native conditions, and analyzed for copurifying proteins by means of SYPRO Ruby stain (Thermo Fisher Scientific). The asterisks indicate the primary translation product, and the arrowheads indicate UBE2O (verified with immunoblotting and mass spectrometry). (**C**) ^{35}S-labeled RPL8 was synthesized in the PURE system and incubated with recombinant E1, ATP, ubiquitin, and UBE2O. (Left) Aliquots of the reaction after different times of incubation at 37°C. (Right) RPL8 was incubated for 60 min at 32°C with E1, ATP, ubiquitin, and the indicated UBE2O variant. (**D**) HEK293 cells stably expressing GFP-RPL24 were treated with three different siRNAs against UBE2O and analyzed by means of flow cytometry. The relative GFP-RPL24 level, normalized to an internal expression control (fig. S10D), is plotted as a histogram. The gray histogram is from cells treated with a control siRNA. (**E**) GFP-RPL24 cells were transiently transfected with plasmids encoding UBE2O, a catalytically inactive mutant (C1040S), or blue fluorescent protein (BFP) (a negative control) and analyzed for GFP-RPL24 levels by means of flow cytometry. (**F**) GFP-RPL24 cells were treated with the indicated siRNAs and analyzed for GFP-RPL24 levels by means of flow cytometry.

directly interact with in vitro–translated 3R (fig. S6). Thus, the CR regions of UBE2O directly recognize exposed hydrophobic patches on 3R and other clients to mediate E2 domain–dependent multimonoubiquitination.

In considering potential physiologic quality control clients of UBE2O, we were struck by its marked up-regulation during erythrocyte differentiation (*14*), hinting that the massive increase in hemoglobin synthesis in pre-erythrocytes might necessitate greater quality control. During adult hemoglobin assembly (fig. S7, A and B), α-globin (also called HBA1) uses α-hemoglobin–stabilizing protein (AHSP) to temporarily shield the interface that is eventually occupied by β-globin (*15*). Several human mutations in α-globin impair interaction with AHSP and cause a variant thalassemia-like disease (*16*). Two such mutants were ubiquitinated at elevated levels compared with wild-type α-globin when translated in a reticulocyte lysate (Fig. 3A). These α-globin mutants interacted directly and specifically with UBE2O, as judged by cofractionation (fig. S7C) and cross-linking (Fig. 3B). AHSP is abundant in reticulocyte lysate (the native context for hemoglobin assembly) (*15*), explaining why nascent wild-type α-globin was not ubiquitinated in this experiment. By contrast, UBE2O ubiquitinated wild-type α-globin in the chaperone-free PURE translation system (Fig. 3C). Recombinant AHSP prevented UBE2O-mediated ubiquitination of wild-type α-globin but was less effective for the mutant (Fig. 3D). Thus, UBE2O appears to recognize unassembled α-globin via the region normally covered by AHSP. Consistent with this, lower levels of ubiquitinated α-globin are observed in reticulocytes from *UBE2O*-null mice (*17*).

Although unassembled α-globin represents a physiologically important UBE2O client, a more general client range is suggested by UBE2O's deep conservation across eukaryotes and broad tissue expression in mammals. We reasoned that as with the α-globin–AHSP system, UBE2O may identify other clients via elements that normally should have engaged a protein biosynthesis factor. Major factors engaged by 3R included IPO5, IPO7, and Importin β (fig. S2A), all of which are involved in nuclear import of ribosomal proteins (*18*). Changing 3R to 3D strongly impaired interaction with both UBE2O and IPO7 (fig. S8A), supporting the idea that they recognize juxtaposed basic and hydrophobic residues, a feature also seen on the surface of α-globin recognized by UBE2O (fig. S8B). We thus investigated whether nascent ribosomal proteins—many of which would contain exposed basic and hydrophobic surfaces—might be UBE2O clients.

We found that several (such as RPL3, RPL8, and RPL24) but not all (such as RPS10) ribosomal proteins were highly ubiquitinated after synthesis in reticulocyte lysate, and the ubiquitinated products cofractionate with UBE2O (Fig. 4A and fig. S9). Affinity purification of these nascent ribosomal proteins showed that UBE2O was a major interactor of each protein that was ubiquitinated but not of RPS10 (Fig. 4B). Reconstitution experiments in the PURE system showed that RPL8 was efficiently ubiquitinated by UBE2O, and that its ubiquitination required the catalytic cysteine of the E2 domain and the CR2 region for efficient recognition (Fig. 4C).

We used a green fluorescent protein (GFP)–tagged RPL24 (fig. S10A) that cannot assemble into ribosomes for steric reasons and is degraded in a proteasome-dependent manner (fig. S10B) to verify its interaction with both UBE2O and IPO7 in cultured cells (fig. S10C). Immunoprecipitation of UBE2O recovered unmodified and monoubiquitinated GFP-RPL24, but not IPO7, suggesting that they do not form a ternary complex (fig. S10D). Catalytically inactive UBE2O(C1040S) also recovered endogenous and exogenous RPL24 (but no detectable ubiquitinated forms), whereas UBE2O(ΔCR2) interacted poorly with RPL24 (fig. S10D). Thus, in vitro and in cells, nascent unassembled ribosomal proteins engage either nuclear import factors or UBE2O. The absence of a ternary complex with IPO7 and UBE2O's capacity to ubiquitinate bound clients suggest that it recognizes the population of nascent ribosomal proteins that fail nuclear import or assembly into the ribosome and targets it for proteasomal degradation.

Using a quantitative flow cytometry assay for GFP-RPL24 degradation (in which red fluorescent protein serves as an expression control) (fig. S10A), we found that three independent small interfering RNAs (siRNAs) that reduce UBE2O by ~90% stabilize GFP-RPL24 (Fig. 4D and fig. S10E). By contrast, overexpression of UBE2O stimulated GFP-RPL24 degradation, whereas overexpression of a catalytically inactive mutant (C1040S) acted as a dominant-negative to increase GFP-RPL24 (Fig. 4E). Knockdown of IPO7 to reduce GFP-RPL24 nuclear import resulted in its increased degradation, suggesting that cytosolic degradation is more efficient than a recently described nuclear quality control pathway for ribosomal proteins (*19*). Cytosolic degradation of GFP-RPL24 was attributable to UBE2O because GFP-RPL24 was stabilized by additionally knocking down UBE2O (Fig. 4F). Thus, UBE2O targets for degradation excess ribosomal proteins in the

cytosol by recognizing elements that are ordinarily bound by nuclear import factors or shielded in assembled ribosomes. Whether the multimonoubiquitination mediated by UBE2O is sufficient for proteasomal degradation, or requires another ligase to build polyubiquitin chains, remains to be determined.

We conclude that UBE2O represents a widely expressed, conserved, and inducible quality control factor that can recognize juxtaposed basic and hydrophobic patches on misfolded, unassembled, and mislocalized proteins. Direct client recognition by UBE2O is analogous to San1p, an unrelated quality control ligase in fungi that also engages clients without a chaperone intermediary (*20*). Whether they have converged on similar mechanisms of client selection remains to be seen (fig. S11). The generic recognition features of UBE2O indicate a broad client range, a property that is apparently exploited for degradation of normal cellular proteins in some contexts (*21*, *22*). When expressed at very high levels, as during erythrocyte differentiation, UBE2O can even drive wide-scale proteome remodeling that includes elimination of intact ribosomes (*17*). In most cells under normal conditions, orphan proteins probably represent the predominant clients for quality control given the large number of abundant multiprotein complexes (*23*, *24*), the challenges of precisely matching expression of different subunits (*25*), and inherent inefficiencies in complex assembly (*1*). Indeed, proteomic analyses indicate that ~10% of all newly made proteins may be orphans that are rapidly degraded (*26*). It is likely that many pathways exist to recognize orphans (*27*) because no single biochemical feature would universally define them. Considering that subunits of many complexes are distributed between different chromosomes, aneuploidy increases the cellular burden of orphans (*28*, *29*), perhaps explaining why the 17q25 genomic region containing Ube2O is amplified in several human cancers, and why UBE2O-deficient mice are resistant to multiple models of cancer (*21*, *22*).

REFERENCES AND NOTES

1. J. W. Harper, E. J. Bennett, *Nature* **537**, 328–338 (2016).
2. S. Wolff, J. S. Weissman, A. Dillin, *Cell* **157**, 52–64 (2014).
3. J. Labbadia, R. I. Morimoto, *Annu. Rev. Biochem.* **84**, 435–464 (2015).
4. R. J. Deshaies, *BMC Biol.* **12**, 94 (2014).
5. T. Hessa *et al.*, *Nature* **475**, 394–397 (2011).
6. M. C. Rodrigo-Brenni, E. Gutierrez, R. S. Hegde, *Mol. Cell* **55**, 227–237 (2014).
7. E. Itakura *et al.*, *Mol. Cell* **63**, 21–33 (2016).
8. X. Zhang *et al.*, *EMBO J.* **32**, 996–1007 (2013).
9. Y. Miyazaki, L. C. Chen, B. W. Chu, T. Swigut, T. J. Wandless, *eLife* **4**, (2015).
10. M. Mariappan *et al.*, *Nature* **466**, 1120–1124 (2010).
11. Y. Shimizu, T. Ueda, *Methods Mol. Biol.* **607**, 11–21 (2010).
12. S. Shao, R. S. Hegde, *Cell* **147**, 1576–1588 (2011).
13. N. Mashtalir *et al.*, *Mol. Cell* **54**, 392–406 (2014).
14. I. Wefes *et al.*, *Proc. Natl. Acad. Sci. U.S.A.* **92**, 4982–4986 (1995).
15. A. J. Kihm *et al.*, *Nature* **417**, 758–763 (2002).
16. X. Yu *et al.*, *Blood* **113**, 5961–5969 (2009).
17. A. Nguyen *et al.*, *Science* **357**, eaan0218 (2017).
18. S. Jäkel, D. Görlich, *EMBO J.* **17**, 4491–4502 (1998).
19. M.-K. Sung *et al.*, *eLife* **5**, e19105 (2016).
20. J. C. Rosenbaum *et al.*, *Mol. Cell* **41**, 93–106 (2011).
21. K. Liang *et al.*, *Cell* **168**, 59–72.e13 (2017).
22. I. K. Vila *et al.*, *Cancer Cell* **31**, 208–224 (2017).
23. N. J. Krogan *et al.*, *Nature* **440**, 637–643 (2006).
24. A.-C. Gavin *et al.*, *Nature* **440**, 631–636 (2006).
25. G.-W. Li, D. Burkhardt, C. Gross, J. S. Weissman, *Cell* **157**, 624–635 (2014).
26. E. McShane *et al.*, *Cell* **167**, 803–815.e21 (2016).
27. Y. Xu, D. E. Anderson, Y. Ye, *Cell Discov.* **2**, 16040 (2016).
28. J. C. Guimaraes, M. Zavolan, *Genome Biol.* **17**, 236 (2016).
29. S. E. Dodgson *et al.*, *Genetics* **202**, 1395–1409 (2016).

ACKNOWLEDGMENTS

We are grateful to M. Skehel and his team for mass spectrometry analysis; V. Bittl, M. Daly, and E. Zavodszky for initial help with flow cytometry assays; M. Rodrigo-Brenni for useful discussions about ubiquitination; S. Shao for useful discussions about preparing complexes in the PURE system; S. Elsasser for bioinformatics advice; and D. Finley for sharing results before publication. This work was supported by the U.K. MRC (MC_UP_A022_1007 to R.S.H.). K.Y. was supported by an Overseas Research fellowship from the Japan Society for the Promotion of Science, a fellowship from the Uehara Memorial Foundation, and a MRC postdoctoral fellowship. Additional data can be found in the supplementary materials.

SUPPLEMENTARY MATERIALS

www.sciencemag.org/content/357/6350/472/suppl/DC1
Materials and Methods
Figs. S1 to S11
References (*30*–*41*)

20 February 2017; accepted 8 June 2017
10.1126/science.aan0178

www.sciencemag.org/content/357/6350/472/suppl/DC1

Supplementary Material for

UBE2O is a quality control factor for orphans of multiprotein complexes

Kota Yanagitani, Szymon Juszkiewicz, Ramanujan S. Hegde*

*Corresponding author. Email: rhegde@mrc-lmb.cam.ac.uk

Published 4 August 2017, *Science* **357**, 472 (2017)
DOI: 10.1126/science.aan0178

This PDF file includes:

Materials and Methods

Plasmids, antibodies, siRNAs

Constructs for in vitro translation in reticulocyte lysate (RRL) were in a pSP64-based vector. Constructs for the human tail-anchored protein Sec61β and its derivatives and have been described (*5–6*, *10*, *30*). Sec61β(ΔTM) lacks the hydrophobic TM domain (see fig. S1A). Sec61β(3R) and Sec61β(3D) contain replacements of three residues within the TMD (see fig. S1A) with Arg or Asp codons, respectively. All of these constructs contain a single native Cys residue in the non-TM region that was exploited for sulfhydryl-reactive crosslinking. Each of the constructs also contains the autonomously folding villin head piece (VHP) domain (*31*) inserted into the flexible N-terminal region of Sec61β to increase the molecular weight of the protein so it migrates slower than the highly abundant hemoglobin present in RRL. Variants that were untagged, tagged at the N-terminus with either a 3X-HA or 3X-FLAG tag, and containing or lacking the VHP domain behaved indistinguishably by in vitro translation and ubiquitination properties. The FLAG-tagged versions were used for affinity purification experiments. Constructs for in vitro translation of Sec61β and Sec61β(3R) in the PURE system were similar, but lacked the VHP domain and contained a C-terminal 3F4 epitope tag instead of an N-terminal 3X FLAG tag. These constructs are in a vector (provided with the PURE system kit from New England Biolabs) that contains a T7 promoter and transcriptional terminator. Human KRAS and rabbit HBA1 (encoding α-globin; 82% identical to human α-globin) were amplified by RT-PCR from human and rabbit total RNA, respectively, and inserted into the SP64 and PURE expression vectors, respectively. KRAS constructs contained the 3X-FLAG tag at the N-terminus, while HBA1 constructs in the SP64 vector contained the 3X-HA tag at the N-terminus. HBA1 constructs for the PURE system were untagged. Mutants of KRAS and HBA1 were generated by site-directed mutagenesis and are described in figs. S3 and S7, respectively. Pre-pro-Cecropin (ppCec) and its Δ6-12 mutant have been described (*12*). These open reading frames were transferred to the PURE vector for expression in that system. Human ribosomal protein coding sequences were either amplified by RT-PCR and cloned into the SP64-based vector, or synthesized as gBlocks (IDT) containing an SP6 promoter for direct use in transcription reactions. These were tagged at the N-terminus with 3X-FLAG. A version of RPL8 was also made in the PURE vector, while RPL24 was engineered into the previously described GFP-2A-RFP mammalian expression plasmid (*7*) for analysis in cells (see fig. S10A). The mammalian UBE2O expression plasmid contains the human UBE2O sequence, amplified by PCR, inserted into a pCDNA3.1-based vector containing a 3X-FLAG tag at the N-terminus. The C1040S mutation was generated by site-directed mutagenesis, while deletion constructs were produced using a PCR-based strategy. ΔCR1 deletes residues 2-450, ΔCR2 deletes residues 502-729, and ΔCC deletes residues 811-882. For expression of domains in E. coli, the CR1 (residues 45-459), CR2 (residues 502-729), and CC (residues 818-882) regions were amplified by PCR and inserted into pGEX-6p1 to generate proteins tagged at the N-terminus with GST. The construct to express recombinant CaM in *E. coli* has been described (*12*). The coding region of rabbit AHSP was amplified by RT-PCR from reticulocyte RNA and cloned into a pGEX-6p1 vector for recombinant expression in E. coli. Commercial antibodies were from the following sources: UBE2O (Bethyl #A301-873A), IPO7 (Bethyl #A302-727A), RPS20 (Abcam #ab133776), RPL24 (Abcam #ab126172) Rabbit anti-BAG6 and anti-GFP have been described(*10*, *30*). GFP-Trap (immobilized camelid nanobody against GFP) was from ChromoTek. Anti-GST was a gift

from M. Machner (NIH). Anti-FLAG and anti-HA affinity resins were from Sigma (#A2220 and #A2095). Pre-designed and validated Silencer Select siRNAs for UBE2O and IPO7 knockdowns were obtained from Thermo Fisher (UBE2O #1 s34219, UBE2O #2 s34220, UBE2O #3 s34221, IPO7 #1 s20639, IPO7 #2 s20640).

Recombinant proteins

Full length UBE2O, UBE2O(C1040S), ΔCR1, ΔCR2, and ΔCC were produced by over-expression in mammalian cells by transient transfection and purified from the cytosol fraction by FLAG affinity chromatography using previously described methods (*5*, *6*). Briefly, constructs encoding Flag-tagged UBE2O variants were transfected into HEK293T cells using TransIT 293 (Mirus). The cells were split 1:2 the day after transfection and used for protein purification a day later. Generally, eight 10 cm dishes of confluent cells were harvested in ice cold PBS and swelled for 15 min in a total volume of 1.5 ml of hypotonic buffer [50 mM Hepes, pH 7.4, 10 mM KAc, 1 mM MgAc2, DTT, PMSF, 1X EDTA-free protease inhibitor cocktail (Roche)], and lysed by mechanical disruption using a glass dounce and pestle. Lysates were spun for 10 minutes at maximum speed in a tabletop microcentrifuge at 4°C and the postnuclear supernatant was adjusted to 50 mM Hepes, pH 7.4, 100 mM KAc, and 2 mM MgAc2. The sample was then incubated with 250 μl of packed anti-Flag affinity resin for 1 hour at 4° C. The resin was washed five times with wash buffer (50 mM Hepes, pH 7.4, 400 mM KAc, and 4 mM MgAc2). Elutions were carried out with 150μl of 0.5 mg/ml 3X Flag peptide in elution buffer (50 mM Hepes, pH 7.4, 100 mM KAc, and 2 mM MgAc2). HA-CaM-TEV-His6 was expressed in the BL21(DE3) strain of E. coli and purified using Ni-NTA (Qiagen) and hydrophobic interaction chromatography (*12*). Clarified bacterial lysate from a 1 L culture prepared in PBS supplemented with 200 mM NaCl and 10 mM imidazole was bound to 4 ml of Ni-NTA resin. After extensive washing with the binding buffer, the bound proteins were eluted with binding buffer containing 250 mM imidazole. The sample was adjusted to 0.25 mM $CaCl_2$, then bound to a 4 ml column of Phenyl-sepharose (GE Scientific). After washing with 100 mM KCl, 20 mM Hepes, pH 7.4, and 0.25 mM $CaCl_2$, the bound CaM was eluted with the same buffer containing 1 mM EGTA. The protein was then incubated with 0.3 mg TEV protease during dialysis against 100 mM KCl, 50 mM Hepes-KOH, pH 7.4, 10% glycerol, 7 mM 2-mercaptoethanol. The dialyzed sample was passed through a 1.5 ml column of Ni-NTA and the flow though sample was collected. Total yield was ~34 mg. GST and GST-tagged proteins were expressed in BL21(DE3) and purified via Glutathione-sepharose (GE Scientific) as follows. Protein expression was induced with 0.5 mM IPTG for 16 h at 16°C when cultures were ~0.4 to 0.6 OD_{600}. Bacterial lysate was prepared by sonication in PBS containing 500 mM NaCl. After clarification by centrifugation, the lysate was applied to a 5 ml column of Glutathione Sepharose (GE Healthcare), washed extensively with the binding buffer, and eluted three successive times with 6 ml each with 0.2 M Tris, pH 8, 150 mM NaCl, and 10 mM reduced glutathione. The sample was dialyzed against 20 mM Hepes pH 7.4, 110 mM KAc, 2 mM $MgAc_2$, and 5 mM 2-mercaptoethanol. The final protein was concentrated by ultrafiltration. Recombinant human GST-UBE1 (E1 enzyme), UBCH5, Ubiquitin, and His-Ubiquitin were from Boston Biochem.

Mammalian in vitro translation

The RRL translation system was prepared as described previously in extensive detail (*32*). In brief, crude reticulocyte lysate was obtained from Green Hectares, treated with micrococcal nuclease (150 units/ml final concentration) for 12 min at 25°C in most cases, and supplemented with total liver tRNA, free amino acids (except methionine), ATP, GTP, creatine phosphate,

creatine kinase, glutathione, spermidine, and Hepes pH 7.4. KAc, and $MgAc_2$ levels were titrated to find the optimal levels for translation, and this pre-assembled mixture was aliquoted and stored at -80 for subsequent use. Translation was initiated by addition of a total in vitro transcription reaction and either ^{35}S-methionine (500 μCi/ml) or unlabeled methionine (40 μM) as needed. In vitro transcription was with SP6 polymerase as described, and utilized PCR products as the template (*32*). The transcription reaction was directly used for translation (constituting 1/20th the total volume) without further purification. Translation reactions were for between 15-60 min depending on the experiment. In experiments where physical interactions were being assessed or complexes were purified for post-translational ubiquitination reactions (e.g., Fig. 1B and fig. S1D), translations were for 15-30 min at 32°C. In experiments where substrate ubiquitination during the translation reaction was being assessed, translation was for 60 min at 32°C. Immediately after translation, the samples were place on ice, and further manipulations (see below) were performed at 0-4°C unless otherwise indicated. In some cases, translation reactions were flash-frozen in liquid nitrogen and stored at -80°C for further analysis at a later time.

PURE in vitro translation

The PURE translation system ("Protein synthesis Using Recombinant Elements) described previously (*11*) was either obtained from New England Biolabs or prepared in-house (*33*) by minor modifications of established procedures. In both cases, translation reaction assembly followed the instructions provided by NEB, but with the inclusion of ^{35}S-methionine. In brief, the translation components were assembled with the appropriate plasmid DNA at 10 ng/μl and ^{35}S-methionine at 1 mCi/ml. Where indicated CaM was included at a final concentration of between ~20-35 μM (0.4 to 0.7 mg/ml), together with 0.2 mM $CaCl_2$. After translation at 37°C for between 30 min to 2 h, the reactions were chilled on ice, and processed for downstream assays as described below. To isolate CaM-substrate complexes, translation reactions (10 μl each) were diluted with an equal volume of ice-cold physiologic salt buffer (PSB: 100 mM KAc, 50 mM Hepes-KOH, pH 7.4, 5 mM $MgAc_2$) and layered onto 50 μl of a 20% sucrose cushion in PSB. The sample was centrifuged at 55,000 rpm in the TLS-55 rotor (Beckman Instruments) for 90 min at 4°C, and the top 30 ul was recovered for subsequent crosslinking and ubiquitination assays. Soluble HBA1 was prepared similarly, although it could also be generated without CaM due to its increased solubility. RPL8 was prepared without CaM as follows. After translation, the 10 μl reaction was diluted two-fold in high salt buffer to adjust the final conditions of the sample to 575 mM KAc, 50 mM Hepes-KOH, pH7.4, 22.5 mM MgAc2. This was then layered on a 70 μl sucrose cushion containing 20% sucrose and PSB plus 500 mM KAc. After centrifugation at 55,000 rpm for 90 min at 4°C in the TLS-55 rotor, the top 30 μl was recovered and used directly in further assays.

Fractionation and crosslinking

Where indicated, translation reactions were fractionated by sucrose gradient sedimentation at 4°C as described previously (*30*). In brief, samples were layered atop manually prepared 5-25% sucrose gradients in PSB. The gradients were either 2 ml or 0.2 ml, on which either 200 μl or 20 μl of sample were layered. Spin conditions were 55,000 rpms in the TLS-55 rotor (Beckman Instruments) for either 5 h or for 2 h 20 m for the large and small gradients, respectively. These were found to equivalent for the respective sized gradients. 11 fractions (of 200 μl or 20 μl each) were removed from the top and put on ice. Where indicated in the figures, samples were treated with 250 μM bis-maleimido-hexane (BMH) for 30 min on ice to initiate sulfhydryl-mediated

crosslinks, or 250 μM di-succinimidyl-suberate (DSS) at 22°C for 30 min to initiate amine-mediated crosslinks. Reactions were stopped with 20 mM 2-mercaptoethanol for BMH and 0.1 M Tris pH 8.0 for DSS before downstream processing.

Affinity purification

To identify factors associated with quality control clients, 600 μl translation reactions in non-nucleased RRL were performed for 15 min (for Sec61β and variants) or 30 min (KRAS and ribosomal proteins), chilled on ice, and centrifuged at 100,000 rpms for 30 min at 4°C in the TLA100.3 rotor (Beckman Instruments). The supernatant was added to 30 μl of FLAG M2 affinity resin pre-washed in physiological salt buffer 2 (PSB2: 130 mM KAc, 25 mM Hepes-KOH, pH7.4, 5 mM $MgAc_2$) and gently mixed at 4°C for 2 h. The resin was washed four times with 1 ml PSB2 and transferred to a new tube after the fourth wash. Residual wash buffer was removed, and the bound samples were eluted two consecutive times with 60 μl of PSB2 containing 0.5 mg/ml 3X-FLAG peptide (Sigma). Each elution was for 45 min at 22°C. Proteins in the pooled eluates were precipitated with trichloroacetic acid (TCA) and analyzed by SDS-PAGE and SYPRO Ruby as indicated in the figure legends. Individual bands of interest were excised and subjected to tryptic digestion and mass spectrometry to identify the protein(s). Analytic reactions to assess interactions by immunoblotting were performed in the same manner at a smaller scale (typically 100 μl translation reactions), with ^{35}S-methionine to monitor substrate synthesis and recovery. For affinity purification of native complexes for analysis of ubiquitination (e.g., Fig. 1B and fig. S1D), the ribosome-free translation reaction or sucrose gradient fraction of interest was affinity purified using 10 μl FLAG affinity resin as described above, but left on the resin without elution for downstream on-bead ubiquitination reactions (see below).

Ubiquitination reactions

To analyze ubiquitination of in vitro translated products from RRL (e.g., fig. S1B), the translation reaction was supplemented with His-tagged Ubiquitin to 10 μM. Following translation (typically for 60 min at 32°C), one-tenth of the reaction was reserved for analysis of total products to verify equal translation levels. The remainder was denatured by 10-fold dilution in 1% SDS, 0.1 M Tris, pH 8, heated to 95 °C for 5 min, cooled, and diluted in Ubiquitin-pulldown buffer [PBS supplemented with 250 mM NaCl, 0.5% Triton X-100, and 20 mM imidazole (or 50 mM for KRAS pulldowns)]. This was then applied to 20 μl Ni-NTA agarose (Qiagen) and mixed for 1.5 h at 4°C. The resin was washed three times in Ubiquitin-pulldown buffer and eluted with 30 μl of SDS-PAGE sample buffer supplemented with 50 mM EDTA). The products were visualized by SDS-PAGE and autoradigraphy.

Ubiquitination reactions of affinity purified client complexes (e.g., Fig. 1B and fig. S1D) were performed on the beads. The washed resin (10 μl) was drained of residual wash buffer and incubated with 12.5 μl of a mixture containing PSB, 1 mM ATP, 10 mM creatine phosphate, 40 μg/ml creatine kinase, 10 μM His-Ubiquitin, 100 nM human GST-UBE1, and 250 nM UBCH5. The reaction was incubated for 30 min at 32°C and terminated by addition of 100 μl of 1% SDS, 0.1M Tris, pH 8. The samples were denatured for 3 min at 95°C, separated from the beads, and subjected to ubiquitin pulldowns via the His tag as described above. An aliquot of the input sample was reserved and analyzed in parallel.

Ubiquitination reactions of PURE system assembled client-CaM complexes were carried out in PSB. One-fifth of the reaction volume was the client-CaM complex, and the remainder of the

reaction volume comprised 1 mM ATP, 10 mM creatine phosphate, 40 μg/ml creatine kinase, 10 μM His-Ubiquitin, and 100 nM human GST-UBE1. In addition, where indicated, E2 (UBCH5 and/or UBE2O) was included at 250 nM and the reaction initiated by adding EGTA to 1 mM and incubating at 32°C for 1 h unless otherwise indicated in the figure legends. The reaction was terminated by adding SDS-PAGE sample buffer and analyzed directly by gel electrophoresis and autoradiography.

Cell culture analyses

To prepare the GFP-RPL24 cell line, the GFP-RPL24-2A-RFP coding region was engineered into the pCDNA5-FRT-TO vector (Invitrogen) and transfected into Flp-In HEK293 T-Rex cells (Invitrogen). Stable integrants were selected as directed by the manufacturer and characterized by flow cytometry for stable expression and doxycycline induction. Where indicated, siRNA treatement was for 72 hours using Lipofectamine RNAiMAX (Thermo Fisher). Transient transfection of plasmids into these cells was with TransIt 293 (Mirus). Flow cytometry analysis of GFP-RPL24 levels, normalized to RFP levels, was as before (*34*). Cell lysis and analysis of protein interactions by co-immunoprecipitation under native conditions was as follows. Cells were swelled on ice in hypotonic buffer containing 20 mM HEPES pH 7.4, 10 mM KAc, 1.5 mM $MgAc_2$, 1 mM DTT, 1 x Protease Inhibitor Cocktail without EDTA (Roche) for 20 min and lysed with 26G needle attached to a syringe. Lysates were clarified by 10 min centrifugation at 4°C at max speed in tabletop centrifuge. Supernatant was adjusted to 50 mM HEPES pH 7.4, 120 mM KAc and 2.5 mM $MgAc_2$. IP was for 2h in cold room with anti-FLAG resin or GFP-Trap. Beads were washed 4 times with 50 mM HEPES pH 7.4, 120 mM KAc and 2.5 mM $MgAc_2$ changing tubes once before last wash. Elution from FLAG beads was performed with 0.25 mg/ml 3xFLAG peptide in wash buffer for 20 min (two sequential elutions were combined). Elution from GFP-Trap was performed with SDS-PAGE sample buffer with boiling for 5 min.

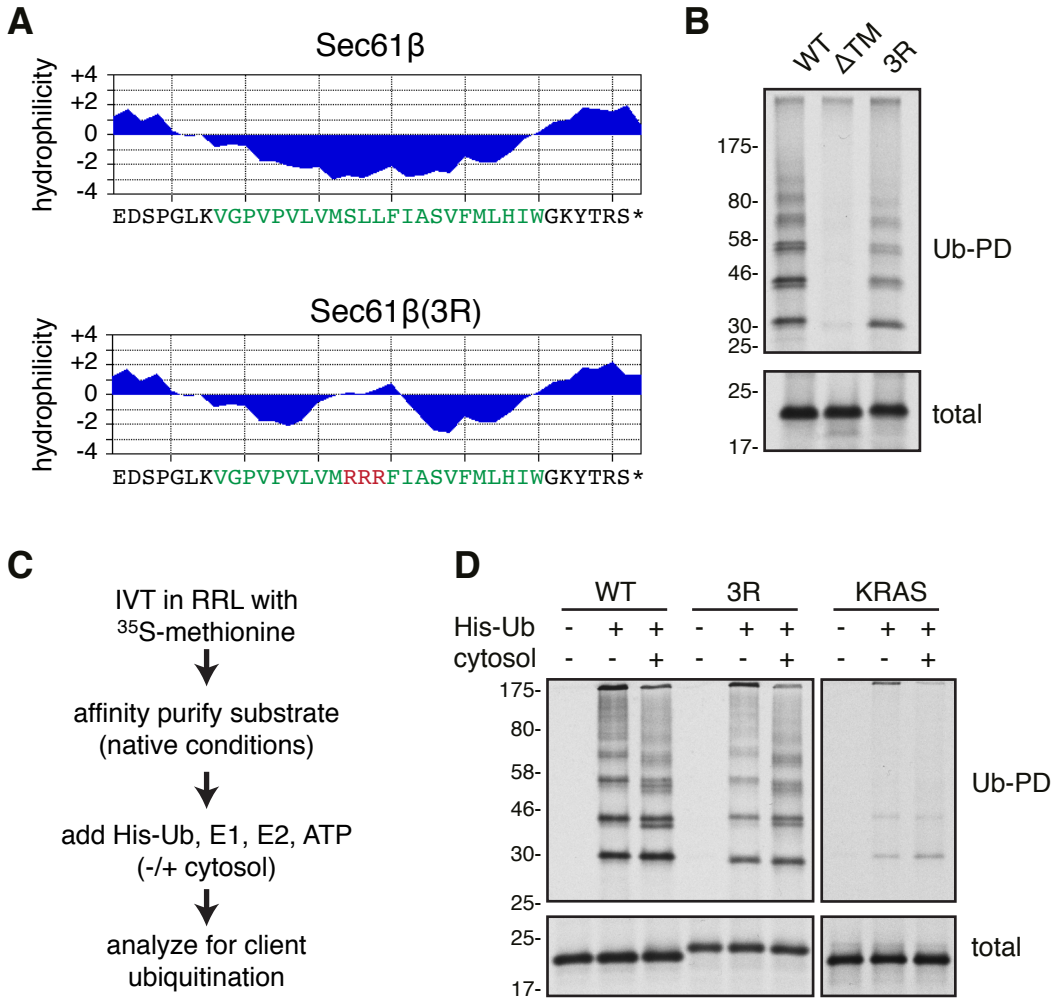

Fig. S1. Sec61β(3R) is ubiquitinated in the cytosol. (**A**) The transmembrane (TM) domain region of Sec61β and Sec61β(3R) are shown, along with their Kyte-Doolittle hydrophilicity profiles. (**B**) Wild type (WT) Sec61β, a mutant lacking the TM domain (ΔTM), and Sec61β(3R) were translated in reticulocyte lysate (RRL) containing His-tagged Ubiquitin and ^{35}S-methionine. One aliquot of each sample was either analysed directly by SDS-PAGE and visualized by autoradiography (total). The remainder was subjected to ubiquitin pulldown (Ub-PD) via the His tag under denaturing conditions, and the ubiquitinated population of the translation product was visualized by autoradiography. (**C**) Experimental strategy to detect the presence of ubiquitination factors stably associated with in vitro translated products. A FLAG-tagged product is translated in RRL for a short time (20 min), when protein synthesis has occurred, but appreciable downstream ubiquitination has not. The translation product is then affinity purified via the FLAG tag under native conditions. The affinity purified sample is then supplemented with ATP, E1, ubiquitin, UBCH5 (E2), and His-Ubiquitin. After incubation, the products are analysed for ubiquitinated client by autoradiography of His-purified products. As a positive control for ubiquitination, cytosol is included in the reaction. (**D**) Analysis of Sec61β, Sec61β(3R), and KRAS by the strategy outlined in panel c. As expected from earlier studies, Sec61β associates with ubiquitination activity (presumably BAG6 and RNF126, as shown before), while KRAS does not associate with appreciable ubiquitination activity as expected for a normal folding protein. The efficient ubiquitination of Sec61β(3R) suggests that it is also associated with ubiquitination machinery. The heterogeneity of ubiquitin bands in the samples with cytosol is due to a mixture of endogenous and His-tagged ubiquitin in the reaction.

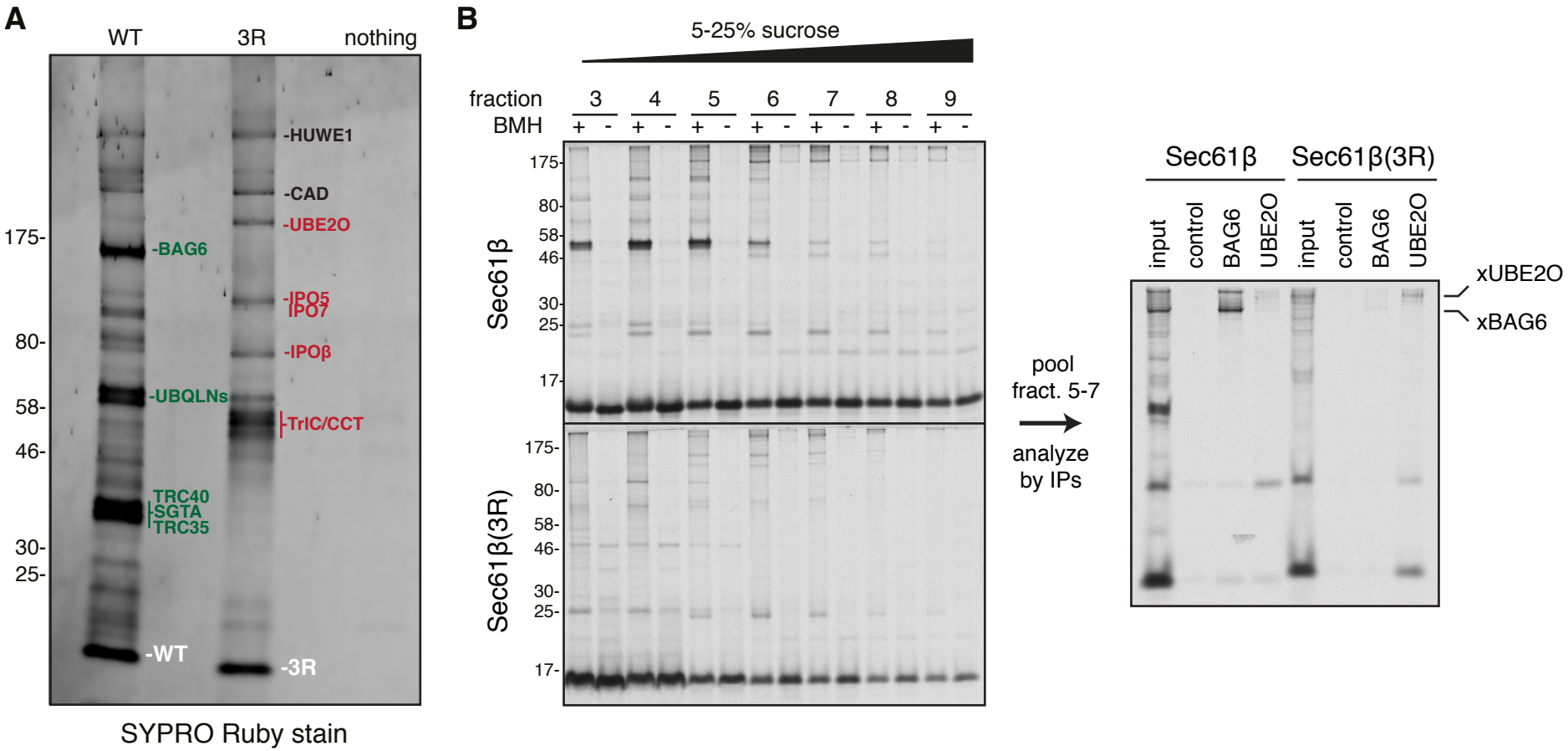

Fig. S2. Identification of UBE2O as a major interaction partner of Sec61β(3R). (**A**) FLAG-tagged wild type (WT) Sec61β, Sec61β(3R), or nothing was translated in RRL and subjected to affinity purification via the FLAG tag under native conditions. The products were analysed by SDS-PAGE and SYPRO Ruby staining. The major bands observed in the WT and 3R samples were excised and identified by mass spectrometry. Proteins specific to 3R (more than three-fold enriched over WT) are indicated in red. Proteins specific to WT are indicated in green, and all represent components of the ER tail-anchored protein targeting pathway. The substrate is indicated in white, while proteins recovered in both samples at comparable levels are indicated in black. (**B**) ^{35}S-labeled Sec61β and Sec61β(3R) were translated in RRL and separated into ten fractions by centrifugation through a 5-25% sucrose gradient under native conditions. The indicate fractions were divided in two, and one was subjected to sulfhydryl-reactive crosslinking with BMH. Both substrates contain a single cysteine at the same position. Fractions 5-7 from the crosslinked samples of each gradient were pooled and either analysed directly (input, right panel), or subjected to denaturing immunoprecipitation using antibodies directed against a control protein (GFP), BAG6, or UBE2O. Sec61β crosslinks prominently with BAG6, but not UBE2O, while Sec61β(3R) crosslinks preferentially with UBE2O, but not BAG6.

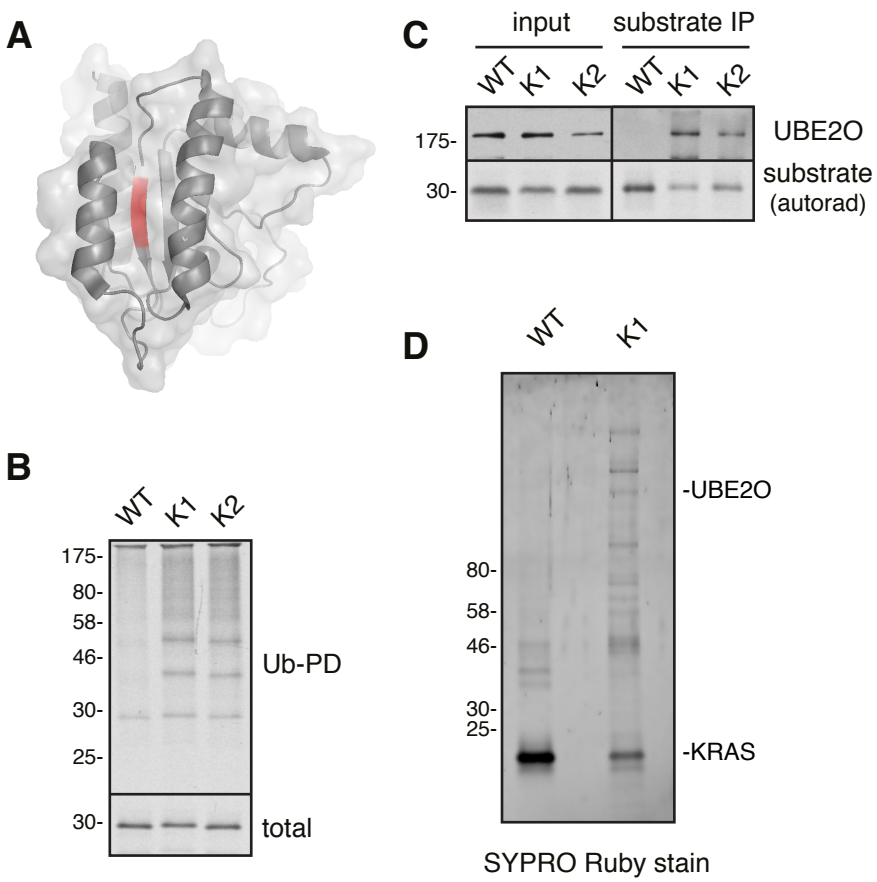

Fig. S3. Misfolded KRAS is ubiquitinated in the cytosol and interacts with UBE2O. (**A**) Structure of human KRAS (PDB 4OBE) with residues 112-114 (encoding Val-Leu-Val) of the buried core indicated in red. These residues were either changed to Arg (to generate mutant K1) or deleted (to generate mutant K2). (**B**) Wild type (WT) KRAS and the mutants K1 and K2 were translated in reticulocyte lysate (RRL) containing His-tagged Ubiquitin and ^{35}S-methionine. One aliquot of each sample was either analysed directly by SDS-PAGE and visualized by autoradiography (total). The remainder was subjected to ubiquitin pulldown (Ub-PD) via the His tag under denaturing conditions, and the ubiquitinated population of the translation product was visualized by autoradiography. (**C**) FLAG-tagged wild type (WT) or mutant (K1 and K2) KRAS were translated in RRL, affinity purified under native conditions via the FLAG tag, and analysed by immunoblotting for UBE2O. The ^{35}S-labeled substrate was visualized by autoradiography. (**D**) FLAG-tagged wild type (WT) or mutant (K1) KRAS were translated in RRL, affinity purified under native conditions via the FLAG tag, and analysed by SYPRO Ruby staining. The band corresponding to UBE2O (identified by mass spectrometry only in the K1 sample) is indicated.

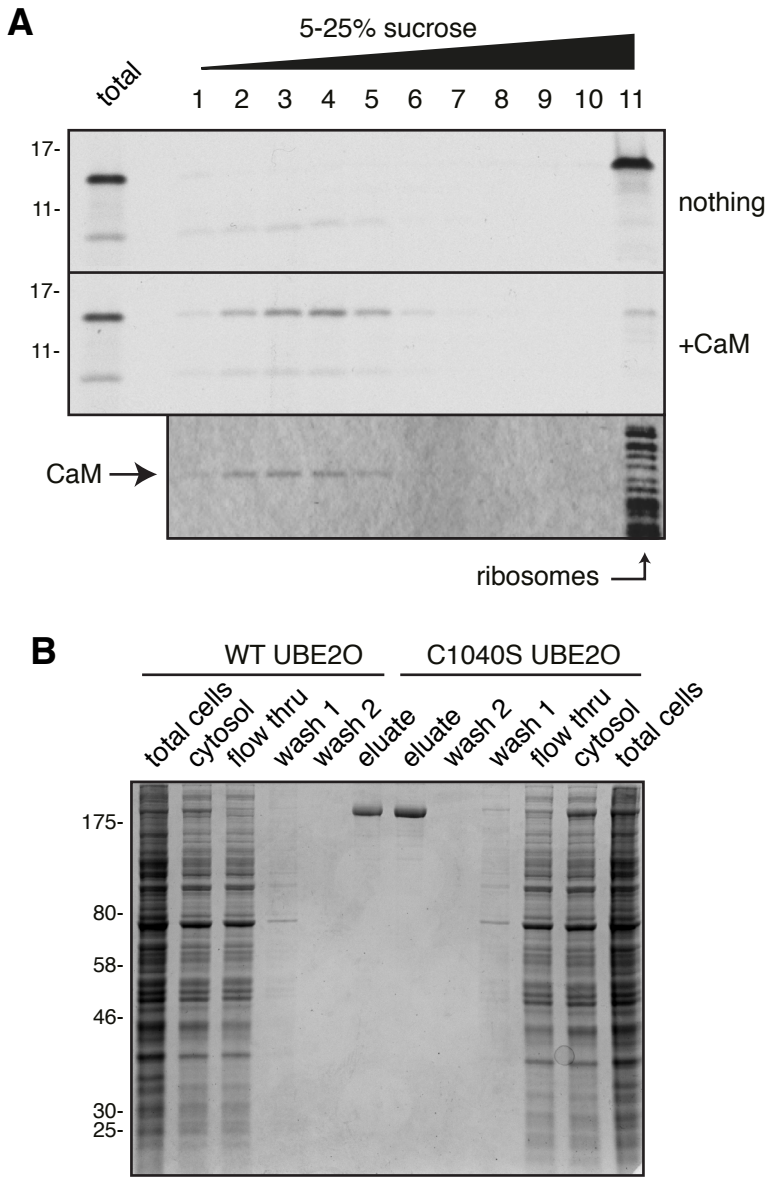

Fig. S4. Preparation of 3R and UBE2O for in vitro ubiquitination assays. (**A**) Sec61β(3R) was translated in the PURE in vitro translation system with ^{35}S-methionine supplemented with no additional factors or with 35 μM Calmodulin (CaM), and was analysed directly (total) or after separation into 11 fractions on a 5-25% sucrose gradient. The ^{35}S-labeled substrate was detected by autoradiography, while CaM was detected by Coomassie staining. Note that Sec61β(3R) quantitatively aggregates (i.e., migrates in the 11th fraction along with ribosomes) without CaM, but is mostly soluble and co-fractionates with CaM when it is present. The peak fractions from such a sucrose gradient fractionation, containing the 3R-CaM complex without any other eukaryotic components, was used for the crosslinking assays in Fig. 2 to characterize the complex. 3R-CaM complexes prepared using a simplified variation of this strategy (see Methods) were used for the ubiquitination assays in Fig. 2 and fig. S5. (**B**) Coomassie stained gel showing the different fractions during the expression and purification of FLAG-tagged human UBE2O and the C1040S mutant in the E2 domain that renders the protein inactive.

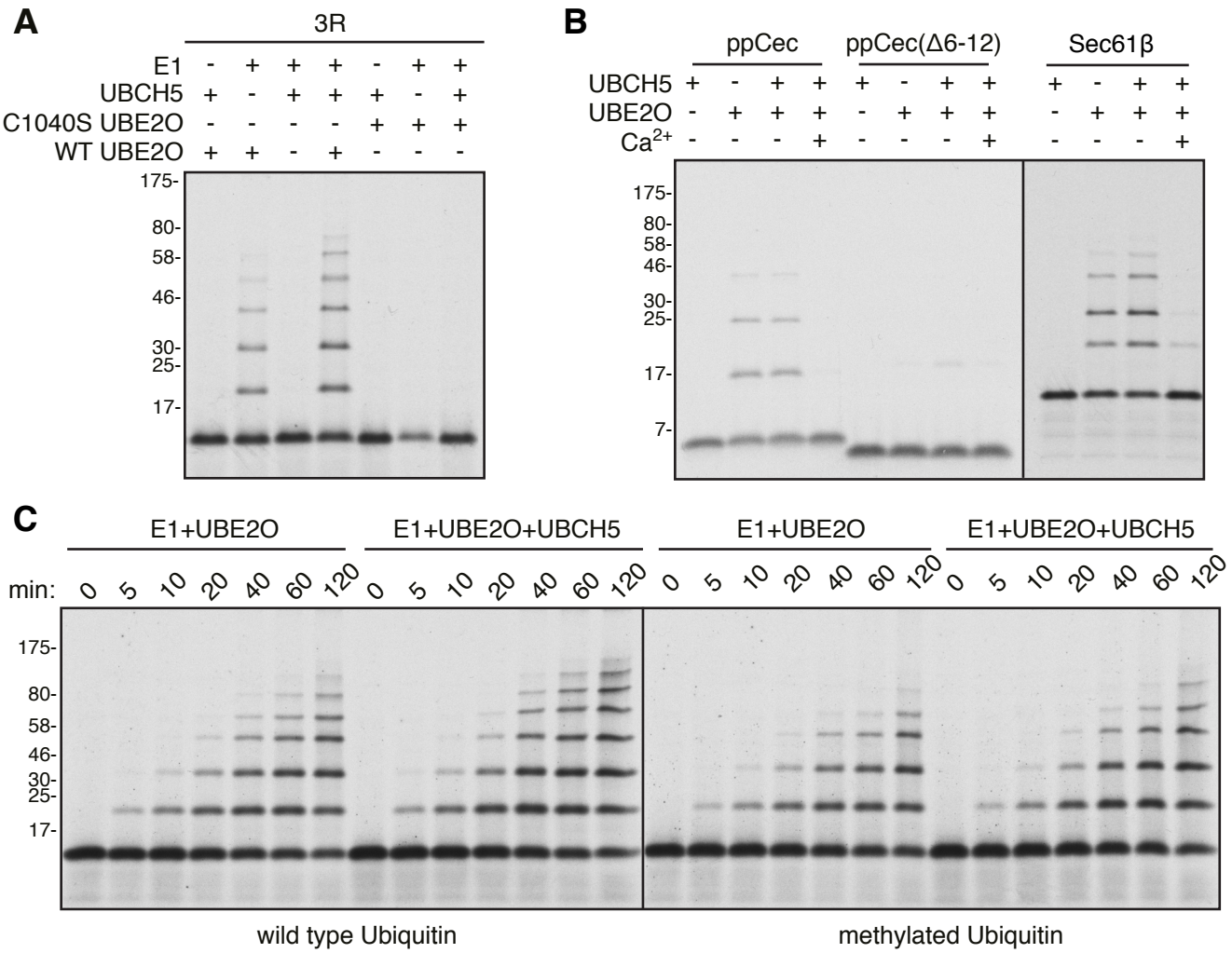

Fig. S5. Characterization of UBE2O-mediated ubiquitination. (**A**) ^{35}S-labeled 3R in complex with CaM was incubated with the indicated factors, ATP, and ubiquitin before analysis by SDS-PAGE and autoradiography. EGTA was added at the beginning of the reaction to 1 mM to induce substrate release from CaM. (**B**) The indicated substrates, prepared as ^{35}S-labeled proteins in complex with CaM as in fig. S4A, were assayed for ubiquitination as in panel A. Where indicated, Ca^{2+} (at 5 mM) was included instead of EGTA to retain substrate on CaM. Cec is pre-pro-cecropin, a secretory protein containing a hydrophobic N-terminal signal peptide. CecΔ6-12 is a mutant that deletes the hydrophobic core of the Cec signal peptide. It is noteworthy that in purified systems, UBE2O can recognize clients of other pathways (e.g., a BAG6 target like Sec61β) that it would ordinarily not engage in cytosol (Fig. 1C). We have made similar observations for BAG6 and Ubiquilins, indicating a considerable amount of plasticity and overlap in substrate range. This property probably provides cells with robustness in dealing with loss or saturation of any one factor, perhaps explaining why cultured cells tolerate the absence of individual pathways surprisingly well (*7*). However, this robustness poses a challenge to identifying the native client range of individual pathways by proteomics of knockout cells, particularly given compensatory mechanisms such as stress response activation (*7*, *9*). For similar reasons, mammalian genetic screens using a quality control client may give muted signals even with bona fide hits. The biochemical strategy of querying a complete cell lysate with tracer quantities of an aberrant protein (e.g., Fig. 1) should provide a general route to identifying the quality control system(s) most optimized for any given client. (**C**) Time course of ubiquitination reactions using 3R as the substrate performed as in panel a. The reaction contained either wild type Ubiquitin or methylated Ubiquitin incapable of forming Ubiquitin linkages. Note that ubiquitination is essentially unimpeded in both speed and number of ubiquitins added to the client with methylated ubiquitin, suggesting that the ladder represents multi-mono-ubiquitination. The substrate contains 6 lysines and the N-terminus, and the maximum number of ubiquitins observed is 7. The slightly lower efficiency with methylated ubiquitin is likely a consequence of its slightly less efficient recognition by E1 and transfer to E2.

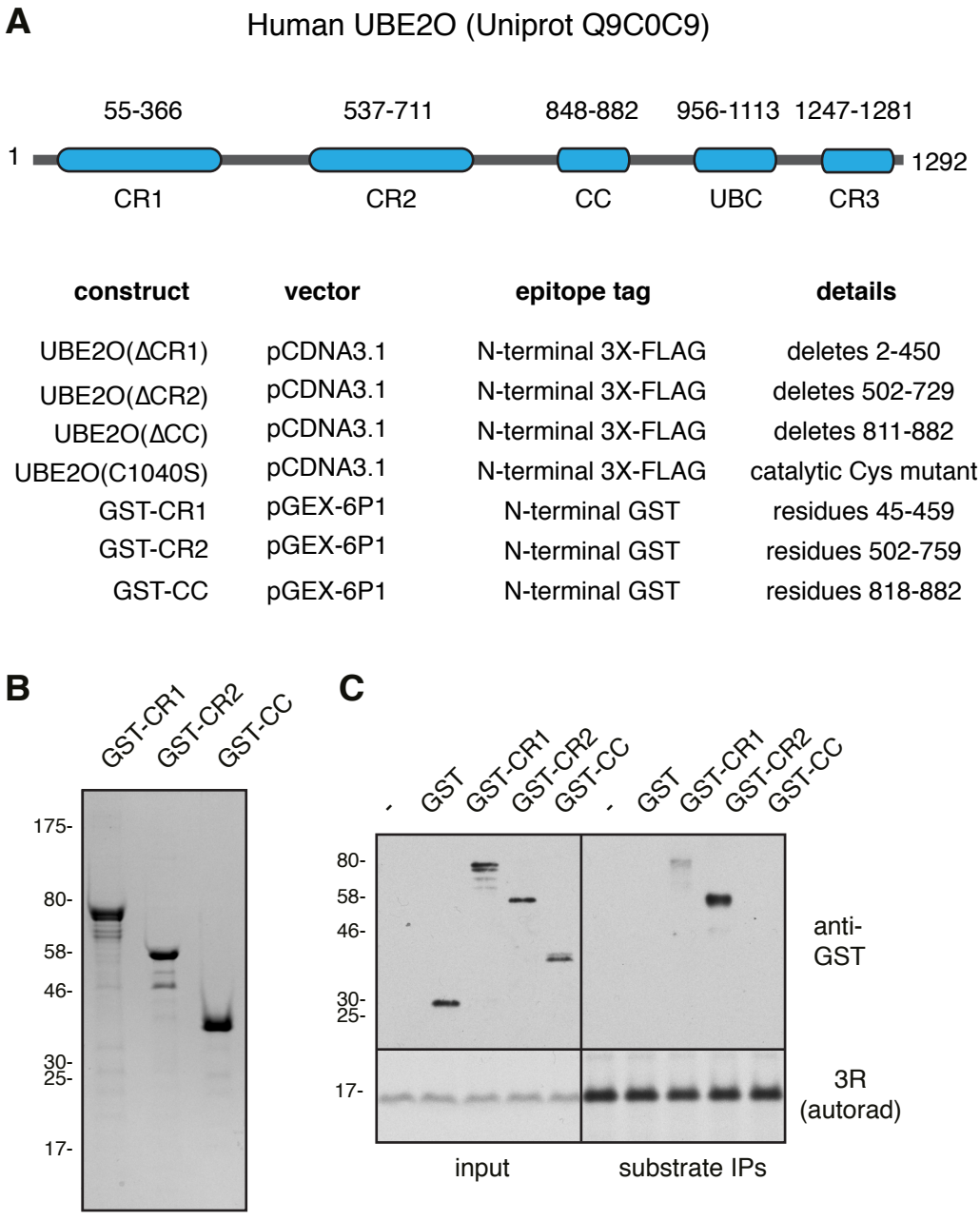

construct	vector	epitope tag	details
UBE2O(ΔCR1)	pCDNA3.1	N-terminal 3X-FLAG	deletes 2-450
UBE2O(ΔCR2)	pCDNA3.1	N-terminal 3X-FLAG	deletes 502-729
UBE2O(ΔCC)	pCDNA3.1	N-terminal 3X-FLAG	deletes 811-882
UBE2O(C1040S)	pCDNA3.1	N-terminal 3X-FLAG	catalytic Cys mutant
GST-CR1	pGEX-6P1	N-terminal GST	residues 45-459
GST-CR2	pGEX-6P1	N-terminal GST	residues 502-759
GST-CC	pGEX-6P1	N-terminal GST	residues 818-882

Fig. S6. Client interaction with different UBE2O domains. (**A**) Line diagram indicating the location and amino acid positions of conserved structured regions (CR1, CR2, and CR3), a predicted coiled-coil (CC) domain, and the UBC domain of UBE2O. Under the diagram is a summary of UBE2O constructs used in this study. (**B**) Coomassie stained gel of purified GST-tagged domains used in the interaction analysis shown in the next panel. (**C**) Purified GST or the indicated GST-tagged proteins were added to RRL at a level twice that of endogenous UBE2O. These supplemented lysates were used for translation of FLAG-tagged 3R, which was affinity purified under native conditions and analysed by immunoblotting with antibodies against GST. The CR2 region interacts most strongly with 3R, with CR1 showing a weaker interaction. Consistent with this observation, ubiquitination assays shown in Fig. 2D show reduced client ubiquitination when CR2 is deleted, and subtle but reproducible decrease when CR1 is deleted.

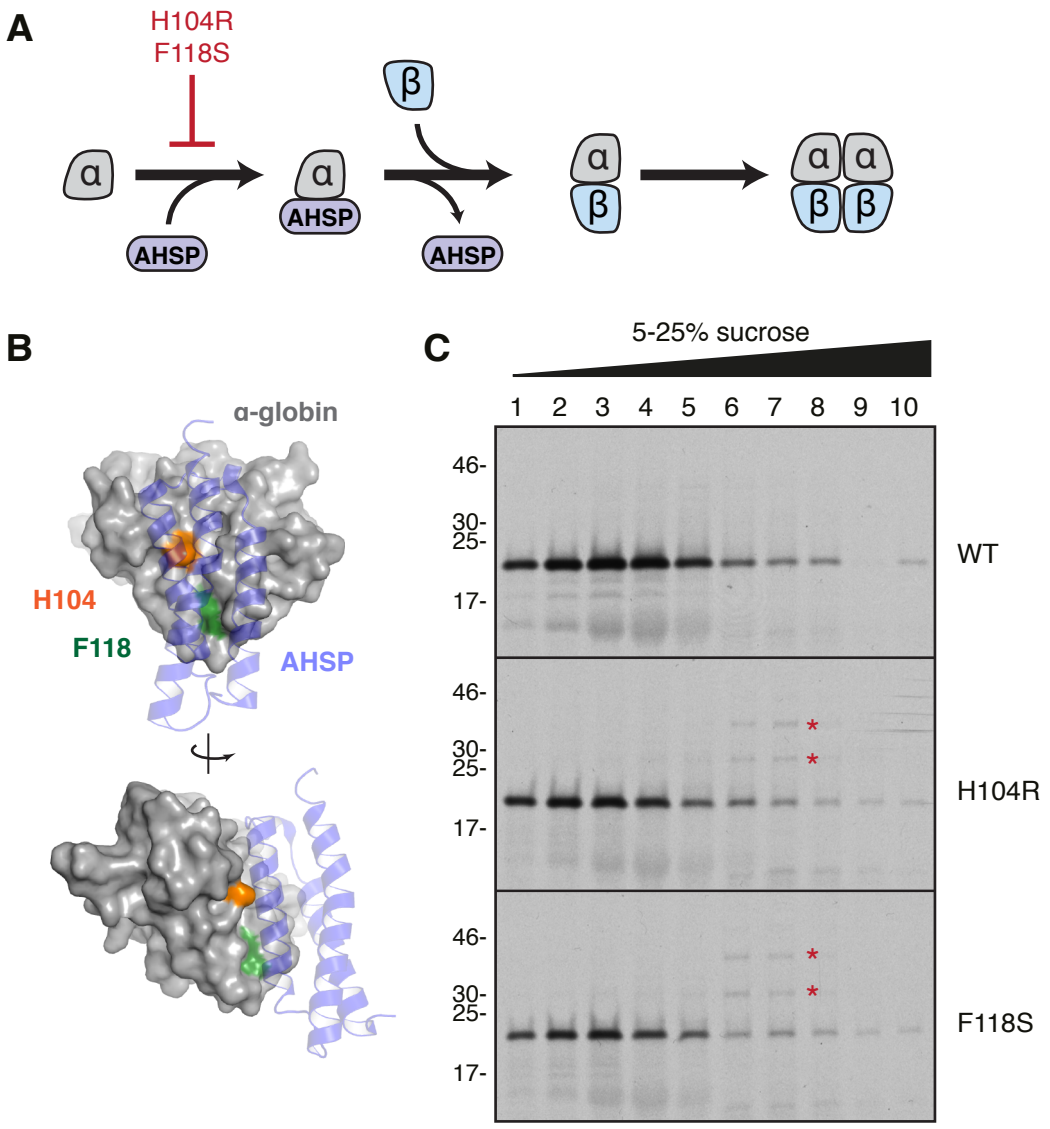

Fig. S7. Characterization of α-globin assembly mutants. (**A**) Simplified schematic of the adult haemoglobin assembly pathway thought to occur in pre-erythrocytes (e.g., reticulocytes). Newly synthesized α-globin engages the highly abundant and reticulocyte-specific chaperone α-hemoglobin stabilizing protein (AHSP) (*15*). β-globin displaces AHSP by binding to the same interface (*35*), after which the α-β associates with another copy of itself to form the mature tetramer. (**B**) Structure of the human α-globin-AHSP complex (PDB ID 1Z8U; ref. *36*) showing globin in grey and AHSP in blue. The positions of two mutations (H104R and F118S) that have been shown to disrupt the α-globin-AHSP interaction (*16*), and thereby impede assembly, are shown in orange and green, respectively. (**C**) HA-tagged wild type (WT) α-globin (also called HBA1) or each of two mutants were synthesized in reticulocyte lysate containing ^{35}S-methionine, separated on a 5-25% sucrose gradient, and visualized by autoradiography. Note that the mutants, but not wild type, becomes ubiquitinated (red asterisks), and that these ubiquitinated products co-migrate in the same high-molecular weight fractions as UBE2O (primarily fractions 6 and 7; see fig. S9A). The physical interaction with UBE2O in these fractions was verified by crosslinking and immunoprecipitation in Fig. 3B.

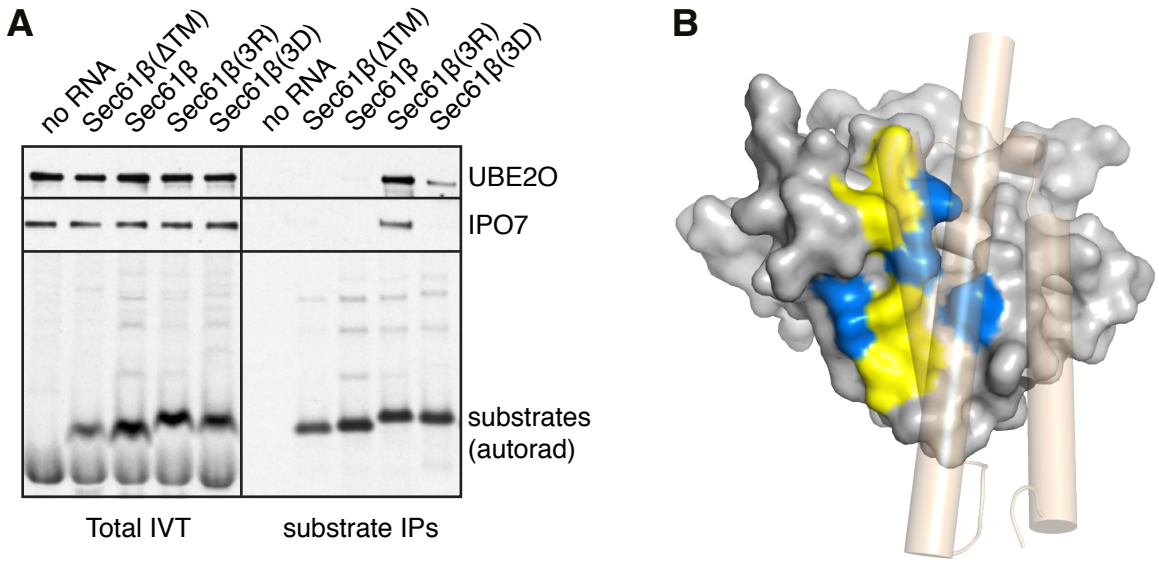

Fig. S8. Basic and hydrophobic residues in the client facilitate UBE2O recognition. (**A**) In vitro translation reactions in RRL containing ^{35}S-methionine and the transcript coding for the indicated FLAG-tagged protein were analysed directly (total IVT) or after affinity purification via the FLAG tag. The substrate was visualized by autoradiography, while UBE2O and Importin 7 (IPO7) were detected by immunoblotting. Sec61β(3D) is identical to 3R except that the three Arginine residues were changed to Aspartates. Note that this substantially reduces interaction with both UBE2O and IPO7. Of note, 3D is still perceived as aberrant in RRL, and is seen to be ubiquitinated. Preliminary analysis suggests that this pathway is different than the UBE2O pathway, but we have not yet identified the responsible machinery. (**B**) Structure of the human α-globin-AHSP complex (PDB ID 1Z8U) showing globin in grey and AHSP in tan. The surface of α-globin occluded by AHSP is colored to show hydrophobic residues in yellow and basic residues in blue. This is the region that is apparently recognized by UBE2O since mutants that prevent AHSP binding favor UBE2O-mediated α-globin ubiquitination (Fig. 3). Considered with the result in panel A, it appears that juxtaposed basic and hydrophobic residues are a key recognition element for UBE2O. Almost all ribosomal proteins are highly basic, and before they are folded and incorporated into ribosomes, also would expose hydrophobic patches. Thus, the artificial protein 3R, unassembled α-globin, and many unassembled ribosomal proteins would share this property, making them targets for UBE2O.

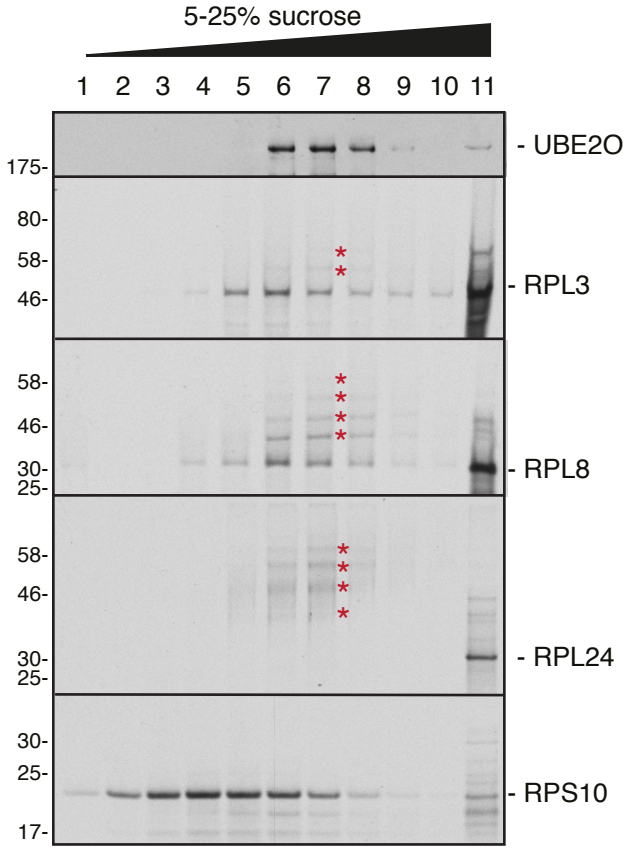

Fig. S9. Several nascent orphan ribosomal proteins co-fractionate with UBE2O. The indicated ribosomal proteins were synthesized in reticulocyte lysate containing ^{35}S-methionine, separated on a 5-25% sucrose gradient, and visualized by autoradiography. Note that RPL3, RPL8, and RPL24, but not RPS10, become ubiquitinated to varying degrees (red asterisks), and that these ubiquitinated products co-migrate in the same high-molecular weight fractions as UBE2O (primarily fractions 6 and 7). The physical interaction with UBE2O was verified by affinity purification and mass spectrometry (Fig. 4B). In the case of RPL24, whose interaction with UBE2O is remarkably robust (Fig. 4B), most of the synthesized protein is ubiquitinated and all of the ubiquitinated products co-migrate with UBE2O. Reconstitution studies in a purified system showed that ribosomal proteins (such as RPL8, shown in Fig. 4C) are very efficiently and heavily ubiquitinated by purified UBE2O. The high number of ubiquitins (relative to 3R, for example; fig. S5) is presumably a consequence the very large number of Lysine residues in RPL8, and not indicative of poly-ubiquitin chains. This is based on the observation that UBE2O in purified assays seems incapable of building ubiquitin chains (fig. S5C).

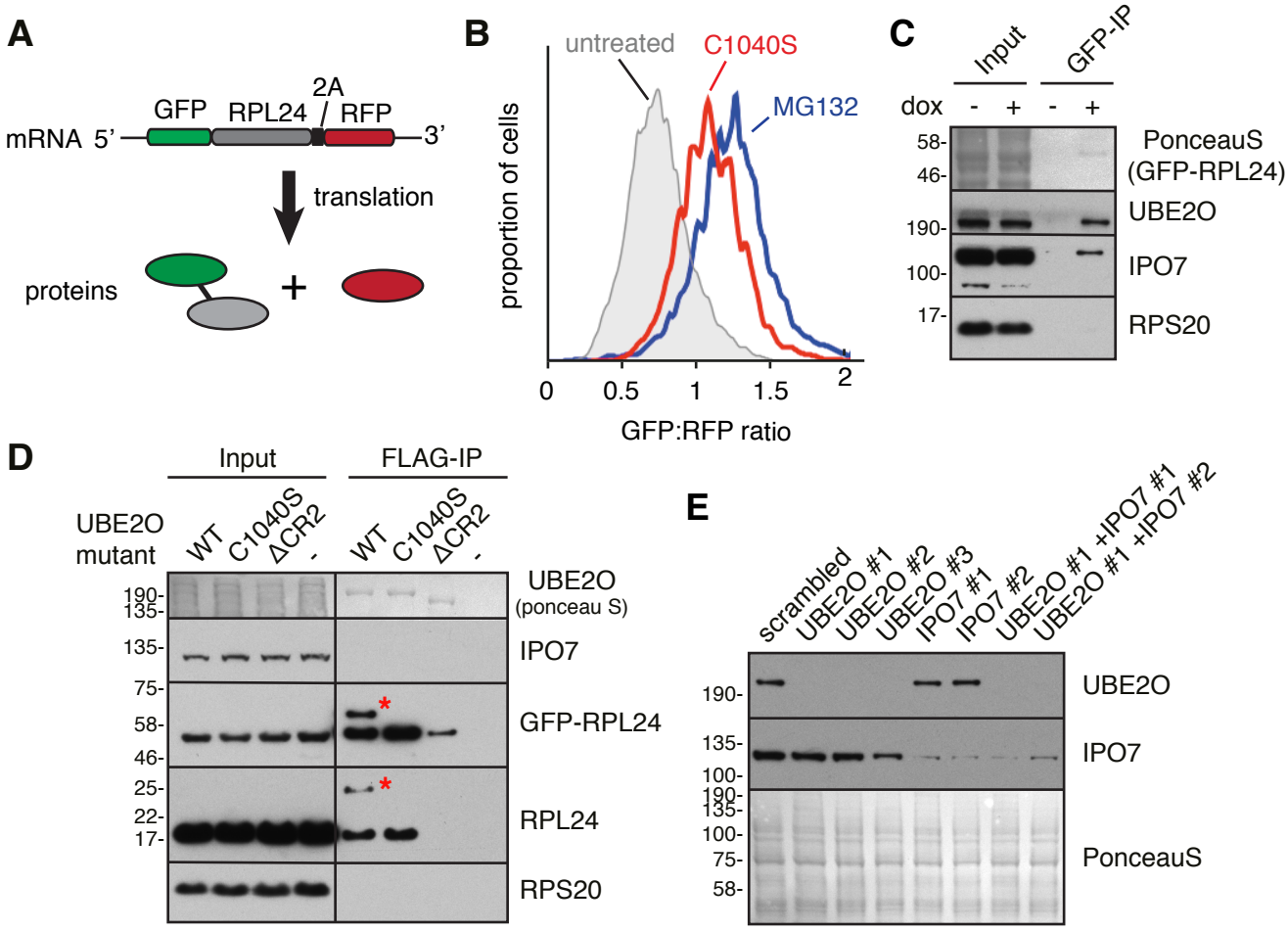

Fig. S10. Additional analysis of UBE2O in cultured cells. (**A**) Schematic diagram of the construct for GFP-RPL24 expression. In this construct, GFP is appended to the N-terminus of RPL24, which in an intact ribosome, would be buried. Thus, GFP-RPL24 cannot assemble into a ribosome properly, and is therefore orphaned. The GFP-RPL24 coding sequence is fused to RFP, but is separated by a viral 2A sequence that skips formation of a peptide bond. This results in translation of two separated proteins from a single mRNA: GFP-RPL24 and RFP, permitting the latter to serve as an expression control for the former. Thus, changes in degradation of GFP-RPL24 will be observed as a change in the GFP:RFP ratio, permitting accurate assessment of GFP-RPL24 levels on a single-cell basis using flow cytometry. (**B**) The GFP-RPL24 construct from panel A was introduced into the FRT site of Flp-In HEK293 TRex cells. The resulting stable cell line was induced for 24 h with doxycycline to drive GFP-RPL24 expression and analyzed by flow cytometry without further treatments or after proteasome inhibition with 20 μM MG132 for 6 h. For comparison, the effect of over-expressing a catalytically inactive dominant-negative UBE2O mutant (C1040S) is also shown. (**C**) The GFP-RPL24 stable cell line was either left uninduced or induced with doxycycline to drive GFP-RPL24 expression. Cell lysates were then subjected to affinity purification using GFP-trap and analzed by total protein staining to visualize GFP-RPL24 (top panel) or immunoblotting for UBE2O, Importin 7 (IPO7) or RPS20 (a negative control verifying that GFP-RPL24 was not incorporated into and recovering whole ribosomes). Earlier studies have shown that IPO7 and IPO5, in addition to acting as import factors, also play a critical role in maintaining ribosomal protein solubility (*37*). Given that UBE2O appears to bind the same regions (and hence, does not form a ternary complex with IPO7 as shown in the next panel), we believe it too is important for preventing aggregation of its clients. (**D**) GFP-RPL24 cells were transfected with the indicated FLAG-tagged UBE2O constructs (or nothing) and subjected to anti-FLAG affinity purification. The recovered UBE2O was visualized by total

Fig. S10 legend, continued.

staining, while IPO7, GFP-RPL24, endogenous RPL24, and RPS20 were detected my immunoblotting. Note that GFP-RPL24 and endogenous RPL24 are recovered with both wild type and C1040S UBE2O, with only wild type UBE2O also recovering mono-ubiquitinated GFP-RPL24 and RPL24 (red asterisks). That these bands indeed represent mono-ubiquitination was verified by their sensitivity to a viral de-ubiquitinase. Thus, as expected from biochemical analyses, UBE2O interacts with unassembled RPL24 and mono-ubiquitinates it in a manner dependent on its catalytic E2 domain. Whether mono- or multi-mono-ubiquitination mediated by UBE2O is sufficient for proteasomal degradation remains to be determined. This possibility seems plausible given earlier studies demonstrating that many proteins can be degraded effectively without ubiquitin chain formation (*38*-*40*). Notably, a proteomic analysis of proteins that are degraded without chain formation showed enrichment for ribosomal proteins (*40*), consistent with the conclusions of our study. (**E**) GFP-RPL24 cells were treated with the indicated siRNAs as for functional assays in Fig. 4D-4F, and analysed for UBE2O and IPO7 by immunoblotting. Knockdown of UBE2O was judged to be better than 90%, while IPO7 was reduced by ~70%. Ponceau S staining shows total protein levels of the lysates as a loading control.

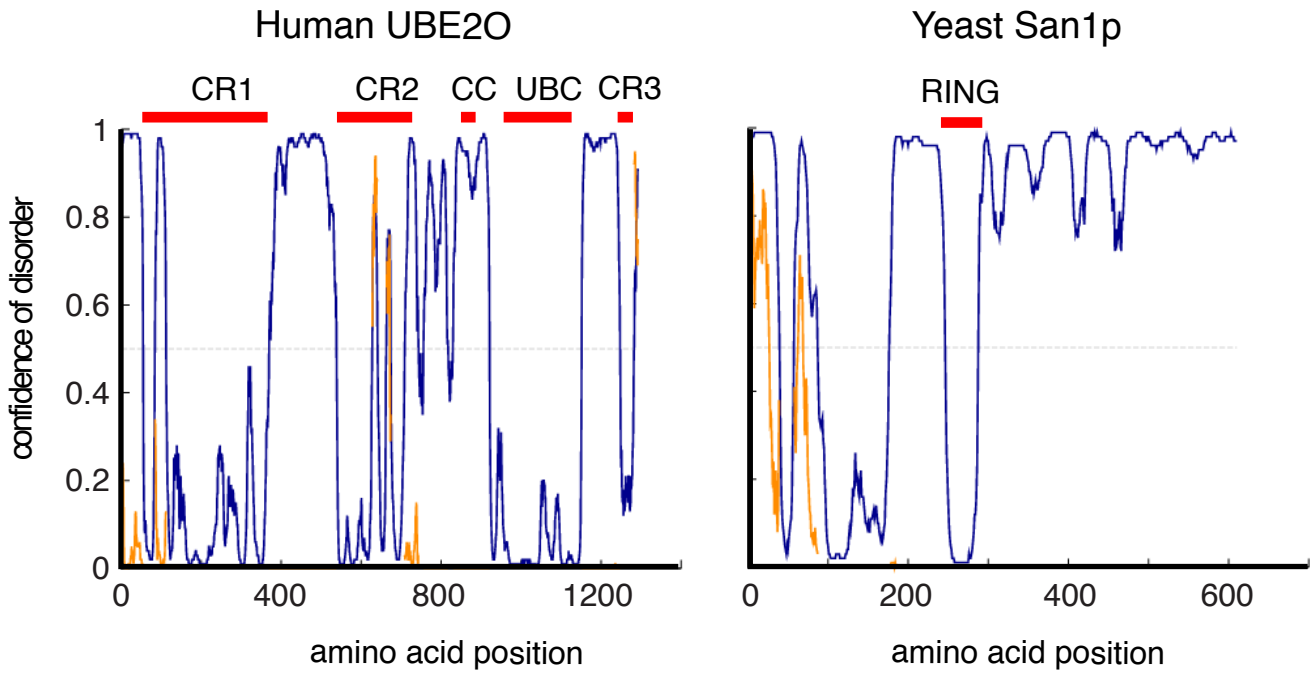

Fig. S11. Comparison of UBE2O and San1p secondary structure predictions. The sequences of human UBE2O and Saccharomyces cerevisiae San1p were analyzed for disordered regions using DISOPRED3 (41). As shown in the blue trace on the plots, the majority of San1p outside of its RING ligase domain is predicted to be disordered. This feature is important for its ability to engage a broad range of substrates (20). By contrast, UBE2O is less disordered overall, with the least disorder observed in the three conserved domains (CR1, CR2, and CR3) and UBC domain. As CR1 and CR2 appear to be involved in substrate binding, it would seen that UBE2O and San1p use different mechanisms of substrate binding. Nevertheless, CR3 and/or the large disordered regions between CR1, CR2, and UBC domains might play a role in binding certain substrates, and this remains to be examined.

References and Notes

1. J. W. Harper, E. J. Bennett, Proteome complexity and the forces that drive proteome imbalance. *Nature* **537**, 328–338 (2016). doi:10.1038/nature19947 Medline

2. S. Wolff, J. S. Weissman, A. Dillin, Differential scales of protein quality control. *Cell* **157**, 52–64 (2014). doi:10.1016/j.cell.2014.03.007 Medline

3. J. Labbadia, R. I. Morimoto, The biology of proteostasis in aging and disease. *Annu. Rev. Biochem.* **84**, 435–464 (2015). doi:10.1146/annurev-biochem-060614-033955 Medline

4. R. J. Deshaies, Proteotoxic crisis, the ubiquitin-proteasome system, and cancer therapy. *BMC Biol.* **12**, 94 (2014). doi:10.1186/s12915-014-0094-0 Medline

5. T. Hessa, A. Sharma, M. Mariappan, H. D. Eshleman, E. Gutierrez, R. S. Hegde, Protein targeting and degradation are coupled for elimination of mislocalized proteins. *Nature* **475**, 394–397 (2011). doi:10.1038/nature10181 Medline

6. M. C. Rodrigo-Brenni, E. Gutierrez, R. S. Hegde, Cytosolic quality control of mislocalized proteins requires RNF126 recruitment to Bag6. *Mol. Cell* **55**, 227–237 (2014). doi:10.1016/j.molcel.2014.05.025 Medline

7. E. Itakura, E. Zavodszky, S. Shao, M. L. Wohlever, R. J. Keenan, R. S. Hegde, Ubiquilins chaperone and triage mitochondrial membrane proteins for degradation. *Mol. Cell* **63**, 21–33 (2016). doi:10.1016/j.molcel.2016.05.020 Medline

8. X. Zhang, J. Zhang, A. Bauer, L. Zhang, D. W. Selinger, C. X. Lu, P. Ten Dijke, Fine-tuning BMP7 signalling in adipogenesis by UBE2O/E2-230K-mediated monoubiquitination of SMAD6. *EMBO J.* **32**, 996–1007 (2013). doi:10.1038/emboj.2013.38 Medline

9. Y. Miyazaki, L. C. Chen, B. W. Chu, T. Swigut, T. J. Wandless, Distinct transcriptional responses elicited by unfolded nuclear or cytoplasmic protein in mammalian cells. *eLife* **4**, (2015). doi:10.7554/eLife.07687 Medline

10. M. Mariappan, X. Li, S. Stefanovic, A. Sharma, A. Mateja, R. J. Keenan, R. S. Hegde, A ribosome-associating factor chaperones tail-anchored membrane proteins. *Nature* **466**, 1120–1124 (2010). doi:10.1038/nature09296 Medline

11. Y. Shimizu, T. Ueda, PURE technology. *Methods Mol. Biol.* **607**, 11–21 (2010). doi:10.1007/978-1-60327-331-2_2 Medline

12. S. Shao, R. S. Hegde, A calmodulin-dependent translocation pathway for small secretory proteins. *Cell* **147**, 1576–1588 (2011). doi:10.1016/j.cell.2011.11.048 Medline

13. N. Mashtalir, S. Daou, H. Barbour, N. N. Sen, J. Gagnon, I. Hammond-Martel, H. H. Dar, M. Therrien, B. Affar, Autodeubiquitination protects the tumor suppressor BAP1 from cytoplasmic sequestration mediated by the atypical ubiquitin ligase UBE2O. *Mol. Cell* **54**, 392–406 (2014). doi:10.1016/j.molcel.2014.03.002 Medline

14. I. Wefes, L. D. Mastrandrea, M. Haldeman, S. T. Koury, J. Tamburlin, C. M. Pickart, D. Finley, Induction of ubiquitin-conjugating enzymes during terminal erythroid differentiation. *Proc. Natl. Acad. Sci. U.S.A.* **92**, 4982–4986 (1995). doi:10.1073/pnas.92.11.4982 Medline

15. A. J. Kihm, Y. Kong, W. Hong, J. E. Russell, S. Rouda, K. Adachi, M. C. Simon, G. A. Blobel, M. J. Weiss, An abundant erythroid protein that stabilizes free alpha-haemoglobin. *Nature* **417**, 758–763 (2002). doi:10.1038/nature00803 Medline

16. X. Yu, T. L. Mollan, A. Butler, A. J. Gow, J. S. Olson, M. J. Weiss, Analysis of human α globin gene mutations that impair binding to the α hemoglobin stabilizing protein. *Blood* **113**, 5961–5969 (2009). doi:10.1182/blood-2008-12-196030 Medline

17. A. Nguyen *et al*., UBE2O remodels the proteome during terminal erythroid differentiation. *Science* **357**, eaan0218 (2017).

18. S. Jäkel, D. Görlich, Importin beta, transportin, RanBP5 and RanBP7 mediate nuclear import of ribosomal proteins in mammalian cells. *EMBO J.* **17**, 4491–4502 (1998). doi:10.1093/emboj/17.15.4491 Medline

19. M.-K. Sung, T. R. Porras-Yakushi, J. M. Reitsma, F. M. Huber, M. J. Sweredoski, A. Hoelz, S. Hess, R. J. Deshaies, A conserved quality-control pathway that mediates degradation of unassembled ribosomal proteins. *eLife* **5**, e19105 (2016). doi:10.7554/eLife.19105 Medline

20. J. C. Rosenbaum, E. K. Fredrickson, M. L. Oeser, C. M. Garrett-Engele, M. N. Locke, L. A. Richardson, Z. W. Nelson, E. D. Hetrick, T. I. Milac, D. E. Gottschling, R. G. Gardner, Disorder targets misorder in nuclear quality control degradation: A disordered ubiquitin ligase directly recognizes its misfolded substrates. *Mol. Cell* **41**, 93–106 (2011). doi:10.1016/j.molcel.2010.12.004 Medline

21. K. Liang, A. G. Volk, J. S. Haug, S. A. Marshall, A. R. Woodfin, E. T. Bartom, J. M. Gilmore, L. Florens, M. P. Washburn, K. D. Sullivan, J. M. Espinosa, J. Cannova, J. Zhang, E. R. Smith, J. D. Crispino, A. Shilatifard, Therapeutic targeting of MLL degradation pathways in MLL-rearranged leukemia. *Cell* **168**, 59–72.e13 (2017). doi:10.1016/j.cell.2016.12.011 Medline

22. I. K. Vila, Y. Yao, G. Kim, W. Xia, H. Kim, S.-J. Kim, M.-K. Park, J. P. Hwang, E. González-Billalabeitia, M.-C. Hung, S. J. Song, M. S. Song, A UBE2O-AMPKα2 axis that promotes tumor initiation and progression offers opportunities for therapy. *Cancer Cell* **31**, 208–224 (2017). doi:10.1016/j.ccell.2017.01.003 Medline

23. N. J. Krogan, G. Cagney, H. Yu, G. Zhong, X. Guo, A. Ignatchenko, J. Li, S. Pu, N. Datta, A. P. Tikuisis, T. Punna, J. M. Peregrín-Alvarez, M. Shales, X. Zhang, M. Davey, M. D. Robinson, A. Paccanaro, J. E. Bray, A. Sheung, B. Beattie, D. P. Richards, V. Canadien, A. Lalev, F. Mena, P. Wong, A. Starostine, M. M. Canete, J. Vlasblom, S. Wu, C. Orsi, S. R. Collins, S. Chandran, R. Haw, J. J. Rilstone, K. Gandi, N. J. Thompson, G. Musso, P. St Onge, S. Ghanny, M. H. Y. Lam, G. Butland, A. M. Altaf-Ul, S. Kanaya, A. Shilatifard, E. O'Shea, J. S. Weissman, C. J. Ingles, T. R. Hughes, J. Parkinson, M. Gerstein, S. J. Wodak, A. Emili, J. F. Greenblatt, Global landscape of protein complexes in the yeast *Saccharomyces cerevisiae*. *Nature* **440**, 637–643 (2006). doi:10.1038/nature04670 Medline

24. A.-C. Gavin, P. Aloy, P. Grandi, R. Krause, M. Boesche, M. Marzioch, C. Rau, L. J. Jensen, S. Bastuck, B. Dümpelfeld, A. Edelmann, M.-A. Heurtier, V. Hoffman, C. Hoefert, K. Klein, M. Hudak, A.-M. Michon, M. Schelder, M. Schirle, M. Remor, T. Rudi, S. Hooper, A. Bauer, T. Bouwmeester, G. Casari, G. Drewes, G. Neubauer, J. M. Rick, B.

Kuster, P. Bork, R. B. Russell, G. Superti-Furga, Proteome survey reveals modularity of the yeast cell machinery. *Nature* **440**, 631–636 (2006). doi:10.1038/nature04532 Medline

25. G.-W. Li, D. Burkhardt, C. Gross, J. S. Weissman, Quantifying absolute protein synthesis rates reveals principles underlying allocation of cellular resources. *Cell* **157**, 624–635 (2014). doi:10.1016/j.cell.2014.02.033 Medline

26. E. McShane, C. Sin, H. Zauber, J. N. Wells, N. Donnelly, X. Wang, J. Hou, W. Chen, Z. Storchova, J. A. Marsh, A. Valleriani, M. Selbach, Kinetic analysis of protein stability reveals age-dependent degradation. *Cell* **167**, 803–815.e21 (2016). doi:10.1016/j.cell.2016.09.015 Medline

27. Y. Xu, D. E. Anderson, Y. Ye, The HECT domain ubiquitin ligase HUWE1 targets unassembled soluble proteins for degradation. *Cell Discov.* **2**, 16040 (2016). doi:10.1038/celldisc.2016.40 Medline

28. J. C. Guimaraes, M. Zavolan, Patterns of ribosomal protein expression specify normal and malignant human cells. *Genome Biol.* **17**, 236 (2016). doi:10.1186/s13059-016-1104-z Medline

29. S. E. Dodgson, S. Kim, M. Costanzo, A. Baryshnikova, D. L. Morse, C. A. Kaiser, C. Boone, A. Amon, Chromosome-specific and global effects of aneuploidy in *Saccharomyces cerevisiae*. *Genetics* **202**, 1395–1409 (2016). doi:10.1534/genetics.115.185660 Medline

30. S. Stefanovic, R. S. Hegde, Identification of a targeting factor for posttranslational membrane protein insertion into the ER. *Cell* **128**, 1147–1159 (2007). doi:10.1016/j.cell.2007.01.036 Medline

31. C. J. McKnight, D. S. Doering, P. T. Matsudaira, P. S. Kim, A thermostable 35-residue subdomain within villin headpiece. *J. Mol. Biol.* **260**, 126–134 (1996). doi:10.1006/jmbi.1996.0387 Medline

32. A. Sharma, M. Mariappan, S. Appathurai, R. S. Hegde, In vitro dissection of protein translocation into the mammalian endoplasmic reticulum. *Methods Mol. Biol.* **619**, 339–363 (2010). doi:10.1007/978-1-60327-412-8_20 Medline

33. S. Shao, M. C. Rodrigo-Brenni, M. H. Kivlen, R. S. Hegde, Mechanistic basis for a molecular triage reaction. *Science* **355**, 298–302 (2017). doi:10.1126/science.aah6130 Medline

34. S. Juszkiewicz, R. S. Hegde, Initiation of quality control during poly(a) translation requires site-specific ribosome ubiquitination. *Mol. Cell* **65**, 743–750.e4 (2017). doi:10.1016/j.molcel.2016.11.039 Medline

35. L. Feng, D. A. Gell, S. Zhou, L. Gu, Y. Kong, J. Li, M. Hu, N. Yan, C. Lee, A. M. Rich, R. S. Armstrong, P. A. Lay, A. J. Gow, M. J. Weiss, J. P. Mackay, Y. Shi, Molecular mechanism of AHSP-mediated stabilization of α-hemoglobin. *Cell* **119**, 629–640 (2004). doi:10.1016/j.cell.2004.11.025 Medline

36. L. Feng, S. Zhou, L. Gu, D. A. Gell, J. P. Mackay, M. J. Weiss, A. J. Gow, Y. Shi, Structure of oxidized α-haemoglobin bound to AHSP reveals a protective mechanism for haem. *Nature* **435**, 697–701 (2005). doi:10.1038/nature03609 Medline

37. S. Jäkel, J.-M. Mingot, P. Schwarzmaier, E. Hartmann, D. Görlich, Importins fulfil a dual function as nuclear import receptors and cytoplasmic chaperones for exposed basic domains. *EMBO J.* **21**, 377–386 (2002). doi:10.1093/emboj/21.3.377 Medline

38. Y. Kravtsova-Ivantsiv, S. Cohen, A. Ciechanover, Modification by single ubiquitin moieties rather than polyubiquitination is sufficient for proteasomal processing of the p105 NF-kappaB precursor. *Mol. Cell* **33**, 496–504 (2009). doi:10.1016/j.molcel.2009.01.023 Medline

39. N. V. Dimova, N. A. Hathaway, B.-H. Lee, D. S. Kirkpatrick, M. L. Berkowitz, S. P. Gygi, D. Finley, R. W. King, APC/C-mediated multiple monoubiquitylation provides an alternative degradation signal for cyclin B1. *Nat. Cell Biol.* **14**, 168–176 (2012). doi:10.1038/ncb2425 Medline

40. O. Braten, I. Livneh, T. Ziv, A. Admon, I. Kehat, L. H. Caspi, H. Gonen, B. Bercovich, A. Godzik, S. Jahandideh, L. Jaroszewski, T. Sommer, Y. T. Kwon, M. Guharoy, P. Tompa, A. Ciechanover, Numerous proteins with unique characteristics are degraded by the 26S proteasome following monoubiquitination. *Proc. Natl. Acad. Sci. U.S.A.* **113**, E4639–E4647 (2016). doi:10.1073/pnas.1608644113 Medline

41. D. T. Jones, D. Cozzetto, DISOPRED3: Precise disordered region predictions with annotated protein-binding activity. *Bioinformatics* **31**, 857–863 (2015). doi:10.1093/bioinformatics/btu744 Medline